

MICROCOPY RESOLUTION TEST CHART  
NATIONAL BUREAU OF STANDARDS-1963-A

UNCLASSIFIED

3

SECURITY CLASSIFICATION OF THIS PAGE

REPORT DOCUMENTATION PAGE

1a. REPORT SECURITY CLASSIFICATION <b>UNCLASSIFIED</b>		1b. RESTRICTIVE MARKINGS n/a	
2a. SECURITY CLASSIFICATION AUTHORITY Public Law 95-224		3. DISTRIBUTION/AVAILABILITY OF REPORT Approved for Public Release: Distribution Unlimited	
2b. DECLASSIFICATION/DOWNGRADING SCHEDULE			
4. PERFORMING ORGANIZATION REPORT NUMBER(S)		5. MONITORING ORGANIZATION REPORT NUMBER(S) <b>AFOSR-TR. 84-0256</b>	
6a. NAME OF PERFORMING ORGANIZATION NORTH TEXAS STATE UNIVERSITY	6b. OFFICE SYMBOL (If applicable)	7a. NAME OF MONITORING ORGANIZATION <i>AFOSR/NP</i> <i>Building 410</i> <i>Bolling AFB, DC 20332</i>	
6c. ADDRESS (City, State and ZIP Code) Dpt. of PHYSICS, P.O. BOX 5368 DENTON TEXAS 76203		9. PROCUREMENT INSTRUMENT IDENTIFICATION NUMBER <b>AFOSR-82-0332</b>	
8a. NAME OF FUNDING/SPONSORING ORGANIZATION AFOSR	8b. OFFICE SYMBOL (If applicable) <i>NP</i>	10. SOURCE OF FUNDING NOS.	
8c. ADDRESS (City, State and ZIP Code) Building 410 Bolling AFB, D.C. 20332		PROGRAM ELEMENT NO. 61102F	PROJECT NO. 2301
11. TITLE (Include Security Classification) Study of VUV Generation by coherent resonant frequency mixing in metal vapors		TASK NO. A1	WORK UNIT NO.

12. PERSONAL AUTHOR(S) Dr. JEAN-CLAUDE DIELS			
TYPE OF REPORT annual	13b. TIME COVERED FROM <u>Oct. 1, 82</u> TO <u>Oct. 31, 83</u>	14. DATE OF REPORT (Yr., Mo., Day) 1984, 1, 30	15. PAGE COUNT 56

SUPPLEMENTARY NOTATION

COSATI CODES			18. SUBJECT TERMS (Continue on reverse if necessary and identify by block number)
FIELD	GROUP	SUB. GR.	

19. ABSTRACT (Continue on reverse if necessary and identify by block number)

>The properties of multiphoton resonances (two, four or more) are exploited to enhance up-frequency conversion rates. Simultaneously, the property of reversibility of coherent interaction is used to minimize the resonant losses (two-photon, four photon absorption). A source of tunable, near bandwidth limited pulses, of more than a millijoule energy per pulse has been developed. A new scheme of computer controlled data acquisition system made it possible to analyse, for the first time, the temporal coherence properties of the amplified pulses (at a rate of 20 pps). The method of interferometric autocorrelation has been applied to the study of multiphoton coherences. Two photon transmission measurements were performed through a heat pipe containing lithium vapor.

20. DISTRIBUTION/AVAILABILITY OF ABSTRACT UNCLASSIFIED/UNLIMITED <input checked="" type="checkbox"/> SAME AS RPT. <input type="checkbox"/> DTIC USERS <input type="checkbox"/>		21. ABSTRACT SECURITY CLASSIFICATION Unclassified	
22a. NAME OF RESPONSIBLE INDIVIDUAL <i>Dr. Schlossberg</i>		22b. TELEPHONE NUMBER (Include Area Code) <i>(202) 767-4908</i>	22c. OFFICE SYMBOL <i>NP</i>

84 04 24 020

AD-A140 800

DTIC FILE COPY

DTIC SELECTE  
MAY 07 1984

GRANT AFOSR - 82-0332

ANNUAL REPORT

AIR FORCE OFFICE OF SCIENTIFIC RESEARCH (AFSC)  
NOTICE OF TRANSMITTAL TO DTIC  
This technical report has been reviewed and approved for public release IAW AFR 190-12. Distribution is unlimited.  
MATTHEW J. KERPER  
Chief, Technical Information Division

I. OBJECTIVES

The primary objective of this work is to design an efficient scheme of up-frequency conversion, to the vacuum ultraviolet. Since our method is to exploit properties of coherent propagation in the presence of multiphoton resonances, a secondary objective is to study multiphoton optical pumping (coherent enhancement of multiphoton excitation), multiphoton absorption and ionization.

We intend to maximize the conversion efficiency by making use of :

- a) multiphoton resonant enhancement,
- b) coherent propagation effects
- c) induced resonances.

II. APPROACH

The main advantage to be gained in working in conditions of coherent propagation (pulses shorter than the phase relaxation time in the vapor) is to minimize the energy lost to the medium. Our approach consists in using a sequence of two pulses with a proper phase relationship. For a resonance of order N, a second pulse out of phase by  $\pi/N$  with the first one, will return the atom to the ground state, hence propagate with minimal attenuation (or with gain) through the medium, and be in optimal condition to stimulate the up-conversion process from the upper state (populated by the first pulse).

The transition probability of the up-conversion process is further enhanced by a proximity of a resonance near the up converted photon frequency  $N\omega + \omega_1$ . In the absence of such a resonance, a "laser induced resonant enhancement" can be created by coupling with intense radiation that particular "virtual level" (at  $N\omega + \omega_1$ ) to a real level of the atom.

Unannounced Justification		<input checked="" type="checkbox"/>
By _____		
Distribution/		
Availability Codes		
Dist	Avail and/or Special	
A-1		



Approved for public release; distribution unlimited.

84 - 04 24 020

The various steps of the research are as follows :

- Development of a picosecond source providing tunable pulses (570-700nm) of 1,5 mJ energy.
- Construction of cells (4 photon resonance in mercury) and heat pipes (2 photon resonance in lithium, single and double heat pipes, and cylindric heat pipes for ionisation measurements).
- Development of a data acquisition system capable of averaging out data as a function of relative phase, delay and amplitude of the exciting pulse sequence. The averaging operations have to be performed at a data rate of up to 20 Hz.
- Measurement of transmission (multiphoton absorption) for a two pulse sequence, as a function of the delay and phase difference between the two pulses, and of the pulse energy. The measurements are to be conducted in dye vapors, lithium vapor and mercury vapor (cases corresponding respectively to a single, double and four photon resonance ).
- Measurements of third and fifth harmonic generation in conditions of optimal multiphoton excitation determined in the previous measurements.
- Simultaneous theoretical analysis of the measurements in progress.
- Implementation of the concept of enhancement by "induced resonances".

### III. STATUS OF THE RESEARCH

#### III.I The source and the Data Requisition system

The development of the source has been completed, providing tunable picosecond pulses of 1,5 mJ energy, at a repetition rate of up to 20 Hz. The laser and associated data acquisition system developed for the experiments of coherent multiphoton propagation are described in a publication (submitted to Applied Optics, included as Appendix A). First we summarize the performances of the system, as described in the latter publication. Next, we will focus on some shortcomings, and describe the solution that are being implemented.

### III.1.1 Amplifier characteristics

We use a three stage amplifier (two pumped transversely, one longitudinally). Coupling between the first stages is minimized by synchronizing the first stage at the leading edge while the second stage is synchronized at the trailing edge of the pump pulse. The amplified spontaneous emission (ASE) after the last stage is approximately 1% of the pulse energy, without the use of any other "isolator" than a direct vision prism between the two first stages.

plified beam, which is essential to perform the critical alignment of the interferometers used for the analysis of time and space coherences.

#### Beam Profile

Careful positioning of the pump beams relative to the amplified beam in the last two stages provides complete control over the spatial intensity distribution, from "square" to "Gaussian".

#### Spatial Coherence

of the amplified pulse is demonstrated by achieving uniform extinction of the beam in a Mack Zehnder interferometer.

#### Temporal Coherence

The measurement of temporal coherence is crucial to the experiments of coherent propagation, and has been used to test the laser sources, the scanning technique, and the data acquisition system. The measurements detailed in Appendix A (ref.1 and 2) indicate that the amplifier does not introduce any phase modulation. The amplified pulse can best be represented by a Gaussian temporal profile with a phase modulation  $\phi(t)$  proportional to the pulse intensity ( $\phi=1.43 E^2$ ). Such a determination cannot be made with conventional spectral measurements, since such a chirp corresponds to an increase in the bandwidth duration product of only 10%.

### III.1.2 Data Acquisition

A Mack Zehnder interferometer is used to create the sequence of two pulses with continuously increasing relative phase and delay (as needed for the experiments of coherent propagation, as well as for the analysis

of pulse coherence). The data acquisition system is needed to resolve two conflicting requirements :

- a) the scanning speed has to be fast enough to ensure continuous frictionless motion of the delay arm (minimum speed : one wavelength /2s) ;
- b) averaging of a large number of data points per wavelength increment of the delay arm, which would require even slower scanning speeds.

The solution that has been first implemented (described in Appendix A pg A8-A10 ref.1,2) is to increase the delay at a regular rate of  $0.16\mu\text{m/s}$ , to divide each fringe by an equal number of phase intervals, and to average data of corresponding phase over a set of ~~for instance~~ 100 fringes.

Despite its shortcomings discussed below, this method enabled us to obtain accurate and simultaneous measurements of intensity and interferometric autocorrelations, and to perform as well nonlinear transmission measurements through lithium vapor.

### III.1.3 Latest improvements

It was established that, while delay increments of  $1000\ \mu\text{m}$  occurred at equal time intervals (of 1h,44min,10s), the translation speed showed unacceptable fluctuations over distances of a few microns. These speed fluctuations cause the data in successive periods to be assigned to the wrong "phase channel", resulting in a decrease of the "phase contrast" (between data corresponding to different "phase settings") to be observed.

Inchworm An "inchworm" was purchased from "Burleigh Instruments", with matching funds from the University. According to the manufacturer's advertisements, this piezoelectrically driven device should enable us to reproducibly scan a delay with increments of only  $0.01\ \mu\text{m}$ . Our measurements instead showed a nonlinearity such that the number of steps/period changed more than 50% over only 5 periods. This approach had to be abandoned.

### Simultaneous measurement of the distance

The problems that arose from the previous approach originate from the use of time rather than space as the primary variable.

The interference maxima (or "in phase sequences") did not occur at equal time intervals because of speed fluctuations. This problem is eliminated if the absolute distance is continuously measured with subwavelength accuracy. This is done by sending a He-Ne laser beam through the same optical delay (Mack Zehnder interferometer) as the picosecond pulses, and monitoring the intensity of the transmitted beam to determine the distance. In order to minimize the computing time, conversion of HeNe fringe intensity to distance was first made by comparing the measurements to a table of  $\cos(\frac{4\pi}{\lambda} Z_1)$  values. The purchase of a new fast arithmetic card for the computer enabled us to define the distance by using directly an arc cos(I) subroutine. The computed distance is used to determine, in each successive wavelength increment, the exact "phase channel" to which a particular data point belongs. The data are next averaged per channel, for a large number of wavelengths, as described in Appendix A (ref. 1 and 2).

### III.2 Heat Pipe and Cell Construction

The rather slow scanning process (circa 15 hours) imposes severe constraints not only on the amplifier chain stability but also on the heat pipe. Obviously the heat pipe has to be perfectly leak tight but in addition the outgassing of the walls has to be continuously and selectively (i.e. without pumping the He buffer gas) eliminated during that 15 h period. Another problem is a condensation of solid lithium at the edges of the hot zone. The resulting accumulation over several hours of an annular ridge of solid was sufficient to obturate the optical path of the original heat pipe. To solve this problem we constructed another (single) heat pipe of 2" inside diameter (instead of 1" for the original one). Two photon propagation measurements (appendix B) could be performed with this heat pipe over extended periods of time. The construction of another double heat pipe (of 2" inner diameter) is about to be completed, to be used for the measurements of harmonic generation in mixtures of lithium and magnesium.

In order to perform comparative measurements of coherent propagation and harmonic generation in conditions of single and four photon resonances, vacuum cells have been constructed for dye vapors (malachite green)

and mercury vapor (for 4 photon transition). Because of the relatively high vapor pressure of these samples, simple pyrex cells have been used, with fused silica or LiF windows. The sealed cells are uniformly heated, with a slightly higher heating power applied to the windows, to prevent condensation.

In order to study the ionisation losses associated with two photon excitation of lithium, a cylindrical heat pipe has been designed and is presently being assembled. The upper and lower halves of this heat pipe are electrically isolated making them useable as electrodes.

### III.3 Theory

The computer controlled data acquisition data acquisition system provides a continuous recording of absorption-versus phase and delay. In order to match this large set of data with the theoretical model, a computer program has been made that simulates the complete experiment <sup>3</sup>(Appendix B). In order to bring the computing time under reasonable limits, the propagation problem has been linearized (thin sample approximation).

A theoretical study of multiphoton excitation under sequential excitation by coherent pulses is detailed in a publication submitted to the Journal of Chemistry and Physics <sup>4</sup>(Appendix C). It is shown that, by using a sequence of identical pulses with well defined phase relationship, one combines the spectral selectivity offered by a regular pulse train, with the high peak intensity of the short pulses, which are needed to excite higher order processes. The case of random pulse sequences is also considered, and shown to offer an accurate method to study the influence of source coherence on a multiphoton process.

### IV. PUBLICATIONS

1. H. Vanherzeele and J.C. Diels, "Coherence Properties of a Picosecond Dye Laser Oscillator Amplifier" Meeting of the Optical Society of America, Symposium on Ultrafast Photophysics, Paper Tu G4 october 1984.
2. H. Vanherzeele, H.J. Mackey, and J.C. Diels, "Spatial and Temporal Properties of a Tunable Picosecond Dye Laser Oscillator Amplifier System", Submitted to Applied Optics.

3. H.VANHERZEELE and J-C DIELS, "Interferometric autocorrelations applied to the study of multiphoton Coherence", submitted to the XIV<sup>th</sup> I.Q.E.C. (Anaheim, C.A., June 1984).
4. J.C. Diels and J. Stone "Multiphoton Ionization under Sequential Excitation by Coherent Pulses", submitted to the Journal of Chem. and Phys.(1983)
5. "Influence of Source Coherence on Multiphoton Ionization"  
J.C. Diels and J. Stone, Laser 82, New Orléans, Déc. 1982.

V. PERSONNEL

Dr J.C. Diels, P.I.

Dr H. Vanherzeele, Research Scientist

D. Ussery, Research Associate

A P P E N D I X A

**Spatial and Temporal Properties of a Tunable Picosecond  
Dye Laser Oscillator-Amplifier System**

H. Vanherzeele  
H. J. Mackey  
J.-C. Diels

North Texas State University  
Center for Applied Quantum Electronics  
Department of Physics  
Denton, Texas 76203

ABSTRACT

We describe a high power picosecond dye laser system, providing tunable 1.5 mJ pulses, with a uniform wavefront and Gaussian spatial profile. With the aid of a computer controlled data acquisition system, we have analyzed for the first time the temporal coherence properties of such a system.

## I. INTRODUCTION

We report the development of a picosecond pulse dye laser oscillator-amplifier system, designed for experiments of resonant coherent propagation [1]. Such experiments put stringent requirements on the properties of the laser system, most of which will be reviewed briefly in section II. We have been able to meet these requirements, using a commercially available synchronously pumped dye laser in combination with a home built amplifier. As we will explain in section III, this amplifier consists of three stages, being pumped by a frequency doubled Nd:YAG laser. The first two stages are pumped transversely, while the last stage is pumped longitudinally. We succeeded in achieving a high gain, while avoiding a build-up of amplified spontaneous emission (ASE), without the use of spatial filters or saturable absorbers. Accurate synchronization of the various pulses, combined with a careful optimization of the pump and amplified beam geometry, ensures that the energy of the pump is channeled into the picosecond pulse rather than into ASE. The advantage of our transverse-longitudinal pumping geometry, over purely longitudinally pumped systems, is the ability to control the spatial beam profile, without compromising the output energy. In section IV, we will present interferometric autocorrelation measurements [2,3], performed for the first time on such a picosecond pulse dye laser oscillator-amplifier system. These measurements, for which a new kind of data acquisition system needed to be developed, show that our amplifier does not change significantly the temporal properties of the dye laser pulses. Preliminary measurements of coherent two photon absorption in lithium demonstrate that this system meets the stringent coherence requirements of a multiphoton coherent propagation experiment.

## II. GENERAL DESIGN CONSIDERATIONS FOR A PICOSECOND PULSE DYE AMPLIFIER

Even though we designed our amplifier for achieving a particular goal (saturation of the 2s-4s transition of lithium at 571.2 nm), the main specifications are desirable requirements for a large number of experiments: (1) high output energy; (2) minimum ASE; (3) good beam quality for interferometric experiments, i.e., uniform beam profile and flat, distortion free wavefronts; (4) no temporal phase modulation effects; (5) both short term (pulse to pulse) and long term stability; (6) availability of a c.w. pilot beam propagating through the system, for the ease of alignment of the target experiment. Each of these requirements dictated one or more basic design features of the amplifier to be built, as we will explain now. (See e.g., ref. 4 and 5, and additional references therein for a theoretical analysis.)

Obviously, a high output energy calls for an optimum use of the pump radiation, which in turn requires the minimum beam diameter, in each amplifier stage, compatible with a maximum unsaturated gain. Maximizing the gain for a given input also requires minimalization of ASE. This can be achieved through: (1) accurate timing of the pump pulse relative to the picosecond pulse to be amplified in each stage, thereby minimizing the overlap between the gain pulse in one cell and the ASE from the adjacent cell; (2) accurate geometrical matching of the pump beam and the picosecond dye laser beam, in order to maximize uniform pump depletion by the latter in each cell; (3) appropriate choice of dyes. The choice of dyes is further limited by our requirement that the system should be transparent for the unamplified dye laser pulses, which serve the purpose of a c.w. pilot beam. This last condition is particularly important in applications which require a critical alignment of the amplified beam. For our applications, the dye laser beam has to be sent first along the axis of an interferometric delay line, and subsequently through a long but narrow heat pipe, an operation that requires a c.w. beam. The requirement of an aberration

free temporal and spatial beam profile imposes the following design features: (1) short dye cells in order to minimize pulse broadening and phase modulation effects due to the solvent [6,7]; (2) the absence of spatial filters and saturable absorbers in order to avoid wavefront distortion in subsequent amplifiers; (3) a choice of solvents to obtain maximum thermal conductivity; (4) careful lateral adjustment of the pump beam in the longitudinally pumped cell, to properly shape the spatial beam profile of the amplified dye laser pulses. Finally, stability requirements put stringent conditions on the pump source for the amplifier: (1) short term stability requires a jitter free synchronization between dye laser and amplifier pump; (2) long term stability merely imposes a constant thermal lens effect for the pump laser.

### III. SYSTEM DESCRIPTIONS

The oscillator is a Spectra-Physics dye laser, synchronously pumped by a Spectra-Physics Ar ion laser, which is actively modelocked at 82 MHz. For the gain medium we use Rh 6G in Ethylene Glycol (concentration  $2 \times 10^{-3}$  M). Although Rh 560 would yield a slightly higher gain at 571 nm, we prefer instead to use Rh 6G because of its better chemical stability. (The Rh 560 solution has to be replaced every week.) Wavelength tuning around 571 nm is achieved with a 3-plate birefringent filter. With a 30% output coupler, this system generates a continuous train of 3.6 nJ pulses with a duration of 6.2 ps FWHM.

Our three stage dye amplifier, sketched in Fig. 1, is pumped by a frequency doubled, Q-switched Nd:YAG oscillator-amplifier (Quanta Ray, DCR-1). This system delivers 280 mJ pulses (530 nm) of 8 ns FWHM, at a repetition rate of 10 Hz. The polarization of this beam is orthogonal to the polarization of the dye laser beam. A 1.5 m optical delay separates the dye laser oscillator from the first amplifying cell, in order to prevent oscillation of the latter with the output mirror of the former.

#### a. Beam Geometry

To prevent ASE from building up between stages, a direct vision prism is inserted between the first and second stage. This is the sole "optical isolator" used in our system, in contrast to other set ups which need in addition saturable absorbers and pinholes [4,8,9]. Particularly important in this respect is the expanding beam geometry throughout the system, not only to increase the effectiveness of the prism in discriminating against ASE, but also to maximize the overall gain of the amplifier. Starting with a diameter of less than 1 mm in the first cell, the beam diameter is increased 3 times in the second cell, and further expanded drastically in the last stage. The latter is inserted between two lenses of a collimating beam expander with an aperture ratio of 5. This particular design configuration of the last stage serves a dual purpose. The expansion of the dye laser beam is required in order to keep the energy density at 571 nm below the saturation energy density. On the other hand, the converging geometry of the pump beam is needed to maintain a sufficient level of excitation, despite absorption in the dye. One should bear in mind that the performance limits of the dye amplifier are defined in the last stage. Indeed, the saturation energy density over the output cross section of the last stage is the maximum energy per pulse that the system can deliver (e.g.,  $1 \text{ mJ/cm}^2$  for Rh 6G) [10]. Because of its large cross section, this last stage requires most of the energy (77%) of the pump laser, while yielding only a low gain (factor 8). Of the remaining pump energy, 7% is used for the first stage (gain:  $10^3$ ), and 16% for the second stage (gain: 50).

#### b. Choice of Dyes

For the transversely pumped stages, we use 1 cm long flow through cells, at Brewster incidence. The best dye candidate for a pump wavelength near 530 nm, is Rh 6G (highest gain at 571 nm, longest lifetime). However, the absorption

band of Rh 6G extends well beyond 571 nm. Therefore, Rh 560 has to be used in the first two stages (where the concentration is necessarily high), in order to get a reasonably large transmission of the unamplified dye laser pulses through the system. It was determined empirically that the following dye combinations in the first and second cell yield the best results (maximum pump depletion, minimum ASE, and acceptable loss at 571 nm): for the first stage, a mixture of Rh 560 and Rh 6G in methanol (respectively  $2 \times 10^{-3}$  M, and  $10^{-4}$  M); for the second stage Rh 560 in methanol ( $10^{-3}$  M). Finally, for the last stage, which is 5 cm long, we use Rh 6G to fully maximize the gain. The solvent in this stage is a 0.5% aqueous solution of Ammonix L.O., to minimize thermal effects. For the small dye concentration in this final stage ( $1.5 \times 10^{-5}$  M), the absorption of the unamplified pulses is negligible.

c. Synchronization

In Section II, we emphasized the need for an accurate and jitter free synchronization, in each stage, between the pump pulse and the dye laser pulse to be amplified. To reach this goal, we use the modelocked drive of the Ar ion laser as an absolute clock. Through direct digital division, this clock signal is scaled down to approximately 10 Hz. Next, this signal is used to interrogate the original clock signal in a logical AND gate, thus providing a 10 Hz reference signal, which is perfectly synchronized with the master clock. A detailed description of the electronic circuit has been published elsewhere [11]. The 10 Hz reference in turn is used to directly trigger the Q-switch, and after an appropriate delay, also the flashlamps of the Nd:YAG oscillator-amplifier. The resulting jitter in the synchronization between the pump pulse and the dye laser pulse to be amplified, is of the order of 1 ns.

To further minimize energy fluctuations of the amplified pulse, due to this small remaining jitter, we synchronize the first stage at the leading edge of

the pump pulse, while the second stage is synchronized at the trailing edge. This procedure further helps in reducing undesirable coupling in ASE between the initial stages.

#### d. Performance of the System

The output energy of our amplifier is circa 1.5 mJ per pulse. Pulse to pulse stability is better than 20%. This is a good result for a chain of amplifiers, none of which being saturated. Using fresh dyes, the long term stability is also good (5% over a period of 10 hours). For an optimum synchronization, the ratio of ASE energy to pulse energy after the last stage, is in the order of a few percent only.

The spatial intensity distribution of the amplified beam has also been examined, using an optical multichannel analyzer (OMA). Because the first two stages are pumped transversely, one does not expect a uniform gain profile through the whole chain. Therefore, one may fear that the amplifier design may not provide a useful and smooth pulse spatial profile. Our measurements instead have shown that, by carefully positioning the pump beams relative to the amplified beam in the last two stages, we can achieve complete control of the profile of the output beam. An example is shown in Fig. 2. With the OMA in the free running mode, no shot to shot variations of this profile were detected.

The quality of the amplifier output was also examined with a Mack-Zehnder interferometer. Complete extinction of the beam over its entire cross section could be achieved, with the interferometer balanced. This demonstrates the absence of wavefront distortion in the amplifier chain.

#### IV. TEMPORAL PROPERTIES OF THE AMPLIFIED PULSES

Equally important for coherent propagation experiments, are the temporal properties of the amplified pulses. We infer these properties from second order

intensity and fringe resolved autocorrelation measurements, using a Mack-Zehnder interferometer [2,3]. The main difficulty involved in these measurements, stems from the fact that the delay arm of the interferometer has to be moved uniformly, with absolute subwavelength accuracy, over a sufficiently long distance. Indeed, the requirement that the motion of the delay arm be continuous, without the discontinuities that would result from the static friction coefficient (being larger than the dynamic one), implies a minimum scanning speed. On the other hand, however, an upper limit for this scanning speed is set by the repetition rate of the amplifier (10 Hz), and the requirement that there be at least twenty to thirty data points per period, in order to resolve individual fringes. Obviously, both requirements are conflicting. Moreover, one has to realize that the remaining pulse to pulse instabilities, will cause large fluctuations on top of second order fringes, thereby washing out the fringe contrast. Averaging out the data over a large number of laser shots, will only further reduce this contrast. To solve these problems, we had to develop an adequate data acquisition system.

#### a. Data Acquisition System

The hardware of our data acquisition system is schematically represented in Fig. 3. About 1% of the amplifier output is used as a reference beam, the remaining part is sent through the interferometer. Both the reference beam and one of the output beams of the interferometer are frequency doubled and digitized after detection by photoconductive p-i-n diodes (UDT 100L). The other output beam of the interferometer is used for two photon coherent propagation experiments in lithium vapor. The electronic discriminator in the reference channel, rejects pulses with either too low or too high U.V. energy. This feature is built in, mainly in view of our target experiment, which depends critically on the pulse energy.

The forementioned problem of smoothing the interference fringes is solved in the software of our data acquisition system. First, errors due to amplitude fluctuations of the pulses, are eliminated by computing the ratio of the signals in channel 2 and 1. Next, while varying the delay in the autocorrelator at a regular speed of 0.16  $\mu\text{m/s}$ , the resulting fringes are partitioned over a large number of sets (each set has typically 100 fringes). Per set, two different averaging processes are performed. On one hand, all data in each set are averaged out, thereby washing out the fringes completely. For a large number of sets, this will yield the conventional 3:1 intensity autocorrelation curve. On the other hand, an average fringe per set is constructed, by averaging out the data in a single periodicity over the whole set. An example is shown in Fig. 4. This averaging process permits one to keep track of small phase shifts over consecutive sets of fringes. For a large number of sets, it yields the fringe resolved 8:1 autocorrelation curve. In this way, one thus obtains during a single experiment, both autocorrelation curves.

#### b. Data Reduction

By fitting the experimental data for both the intensity and the fringe resolved autocorrelation curves, it is possible to determine accurately the temporal properties of the amplified pulses. From the experimental set up described above, we obtain two recordings of second harmonic signal versus delay: the intensity and the interferometric autocorrelation. The intensity autocorrelation curve provides a first estimate of a reasonable pulse shape and pulse duration, which is used as a starting point in attempting to fit the interferometric autocorrelation measurements. For a given trial function for the complex electric field envelope

$$\tilde{E}(t) = E(t) e^{i\phi(t)} \quad (1)$$

a numerical computation is made of the interferometric second order autocorrelation

$$F(\tau) = \frac{\int |[\bar{E}(t) + \bar{E}(t-\tau) e^{-2\pi i\nu\tau}]|^2 dt}{2 \int |\bar{E}(t)|^4 dt} \quad (2)$$

of which the intensity autocorrelation  $I(\tau)$  is the subpart, excluding the rapidly varying terms in  $\cos(2\pi\nu\tau)$  and  $\cos(4\pi\nu\tau)$  of (2):

$$I(\tau) = \frac{1 + 2 \int |\bar{E}(t)|^2 |\bar{E}(t-\tau)|^2 dt}{\int |\bar{E}(t)|^4 dt} \quad (3)$$

The computations are organized as follows: first, at  $\tau = 0$ , and at  $\tau = 1/2\nu$  the first fringe maximum and minimum is computed; subsequently,  $\tau$  is incremented by  $\Delta\tau = 1/\nu$ , to generate the next pair of points, and so on. In order to improve the accuracy, an additional loop generates near each fringe maximum three points of  $F(\tau)$ , not more than two of them being located at the same side of that maximum. With a parabolic fit through these points, the computer determines: (1) the true location of that maximum ( $\tau_{\max}$ ), (2) the correct  $\Delta\tau$ , which will be used to initiate the next main loop, (3) the location of the fringe minimum ( $\tau_{\min}$ ), and finally (4) the corresponding values of  $F(\tau_{\max})$ ,  $F(\tau_{\min})$  and  $I(\tau_{\max})$ . Once  $I(\tau)$  and both envelopes of  $F(\tau)$  are computed in this way, the pulse parameters (shape, asymmetry, width, and chirp) are adjusted, until a good fit with the experimental data can be reached. Finally, for the best fitting pulse, the deviation of the average frequency

$$\langle \dot{\phi}(t) \rangle = \frac{\int \dot{\phi}(t) |\bar{E}(t)|^2 dt}{\int |\bar{E}(t)|^2 dt} \quad (4)$$

and the pulse bandwidth

$$\Delta\nu = \sqrt{\frac{\int \dot{\phi}^2(t) |\bar{E}(t)|^2 dt}{\int |\bar{E}(t)|^2 dt} - \langle \dot{\phi}(t) \rangle^2 + \frac{\int |\dot{\bar{E}}(t)|^2 dt}{\int |\bar{E}(t)|^2 dt}} \quad (5)$$

are obtained.

c. Results: Pulse Characteristics Before and After Amplification

Fig. 5a shows the intensity autocorrelation curve for the amplified pulses (dashed line). The solid line represents a numerical fit, using a Gaussian pulse shape with 6.2 ps FWHM (i.e., 5.27 ps  $\text{HW}(1/e^2)\text{M}$ ). Notice that an intensity autocorrelation cannot effectively distinguish between a Gaussian and a Sech pulse shape.

From Eq. (3), it is clear that the intensity autocorrelation is phase independent, and therefore does not carry any information about the pulse chirp. On the other hand, as shown in ref. [2,3], the interferometric autocorrelation is sensitive to the pulse chirp  $\phi(t)$ . The experimental results, obtained for the latter with our amplified pulses, are shown in Fig. 5b (dashed line). The solid line in Fig. 5b represents again the best theoretical fit: Gaussian pulses (6.2 ps FWHM) with a phase modulation proportional to the pulse intensity ( $\phi = 1.43 E^2$ ). For comparison, the 8:1 autocorrelation curve for the same Gaussian pulses, but having instead a linear phase modulation (best fit:  $\phi = 1.5 (t/5.27)^2$ ) is also shown in Fig. 5b (dotted line). As a result, the amplified pulses are not completely bandwidth limited; according to Eq. (5), the bandwidth is 79 GHz.

The data shown in Fig. 5b are much more sensitive to phase modulation effects than, e.g., spectral data. The bandwidth-duration product for the nonlinear chirped pulses in our case is 0.49, or only 10% larger than the minimum of 0.44 for unchirped Gaussian pulses. On the other hand, the FWHM of the upper envelope of the interferometric autocorrelation curve for our pulses is 7.2 ps, compared to 9.5 ps for unchirped pulses; the lower envelope is even more sensitive to phase modulation effects: its FWHM changes by almost 50% from our chirped pulses (9.5 ps) to the case of unchirped pulses (14.7 ps).

The kind of chirp we have detected for the amplified pulses, i.e., a chirp proportional to the time derivation of the pulse intensity, is typical for self-phase modulation of the pulses. An interferometric autocorrelation of the unamplified dye laser pulses, as shown in Fig. 6, clearly indicates that the origin of the chirp is in the laser oscillator, rather than in the amplifier chain. As a matter of fact, partial chirp compensation is taking place in the amplifier: the interferometric autocorrelation curve for the unamplified pulses reveals a phase modulation which is proportional to  $1.84 E^2$  (rather than  $1.43 E^2$  for the amplified pulses).

To conclude, our interferometric autocorrelation measurements, such as shown in Fig. 5b, have demonstrated that the phase distortion introduced by the amplifier is small in the time as well as in the space domain. A peak to background of 8:1 can only be obtained with spatially coherent pulses. Indeed, at zero delay, the maximum signal of eight times the background, requires that the two halves of the pulse interfere constructively over their entire cross section.

## V. CONCLUSIONS

In summary, we have developed a picosecond pulse dye laser oscillator-amplifier system, tunable near 570 nm. At a repetition rate of 10 Hz, the output consists of 1.5 mJ pulses. Both the short term and long term stability is excellent. Contrary to other similar systems, we have avoided the use of either pinholes or saturable absorbers. Therefore, our system requires fewer components, which makes the alignment easier. Despite the absence of pinholes and saturable absorbers, the ratio of ASE energy to pulse energy after the last stage is only a few percent. An additional advantage of our system over other short pulse amplifiers, is the fact that the unamplified dye laser pulses are transmitted through the system, thus providing a c.w. pilot beam. This is an

important feature for applications requiring a critical alignment. Our amplifier output has a uniform spatial beam profile, and distortion free wavefronts. The temporal properties of the amplified pulses have also been investigated, using a computerized data acquisition system, specially developed for this purpose. The pulses are Gaussian (FWHM: 6.2 ps), and present a nonlinear chirp ( $1.4 \text{ E}^2$ ). The bandwidth is 79 GHz. It was shown that the origin of the chirp is in the dye laser oscillator, rather than in the amplifier chain.

#### Acknowledgements

The authors would like to acknowledge the valuable assistance of D. Maxson, who interfaced the detection system to the microprocessor. H. Vanherzeele is on leave from the University of Brussels; he acknowledges financial support from the N.F.W.O. for travel expenses. This research was supported by AFOSR under contract number 82-0332.

## REFERENCES

1. J.-C. Diels and A. T. Georges, *Phys. Rev.* A19, 1589 (1979).
2. J.-C. Diels, E. W. Van Stryland, and D. Gold, *Picosecond Phenomena*, eds. C. V. Shank, S. L. Shapiro and E. P. Ippen (Springer-Verlag, 1978), p. 117.
3. J.-C. Diels, I. C. McMichael, J. J. Fontaine, and C. Y. Wang, *Proceedings of the 3rd Int. Conf. on Picosecond Phenomena*, 116, Springer-Verlag, Berlin (1982).
4. A. Migus, C. V. Shank, E. Ippen, and R. L. Fork, *IEEE J. Quant. El.*, QE-18, 101 (1982).
5. G. Haag, M. Munz, and G. Marowsky, *IEEE J. Quant. El.*, QE-19, 1149.
6. Y. Ishida, K. Naganuma, and T. Yajima, *CLEO-83*, paper ThQ2 (1983).
7. W. Dietel, J. J. Fontaine, and J.-C. Diels, *Opt. Comm.*, 8, 4 (1983).
8. J. L. Martin, R. Astier, A. Antonetti, C. A. Minard and A. Orszag, *C. R. Acad. Sc. Paris*, t.289 (1979).
9. R. L. Fork, C. V. Shank, and R. T. Yen, *Appl. Phys. Lett.*, 41, 223 (1982).
10. P. Hammond, *IEEE J. Quant. El.*, QE-16, 1157 (1980).
11. J. Menders and J.-C. Diels, *Rev. Sc. Instr.*, 53, 1093 (1983).

## FIGURE CAPTIONS

Figure 1. Schematic representation of the three stage amplifier (DBS = dichroic beam splitter, POL = polarizing beam splitter, P = direct vision prism).

Figure 2. Spatial profile of the amplified beam.

Figure 3. Data acquisition system: hardware.

Figure 4. Example of an average fringe, representing a set of fringes.

Figure 5. Experimental results and best theoretical fits for (a) the intensity autocorrelation curve and (b) the fringe resolved autocorrelation curve (dashed lines are experimental curves, solid lines represent the theoretical fits; for the dotted line in (b), see text).

Figure 6. Interferometric autocorrelation curve for the unamplified pulses (the solid line represents the best fit; the dashed line corresponds to the best fit for the amplified pulses).

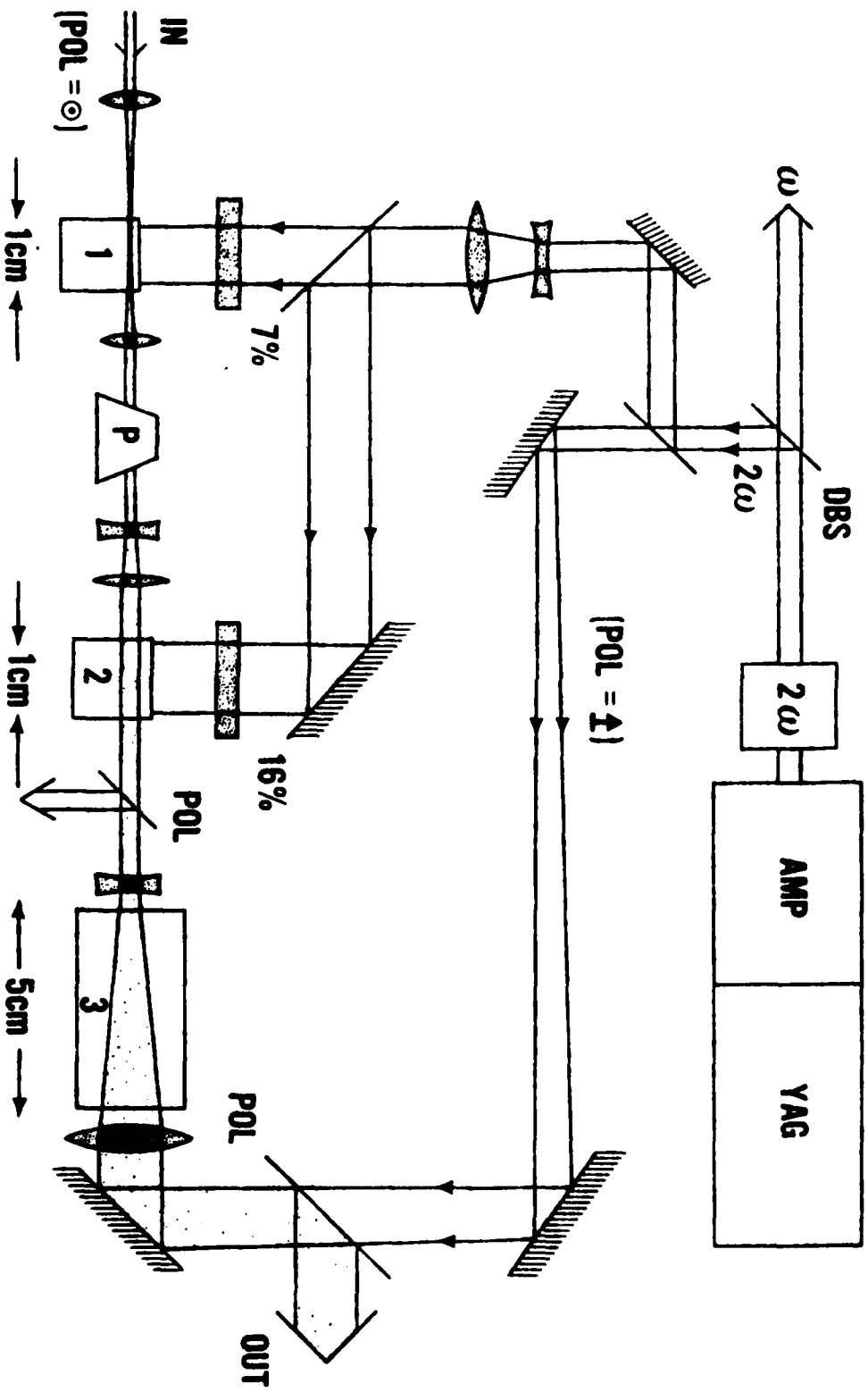


FIGURE 1.

FIGURE 2.

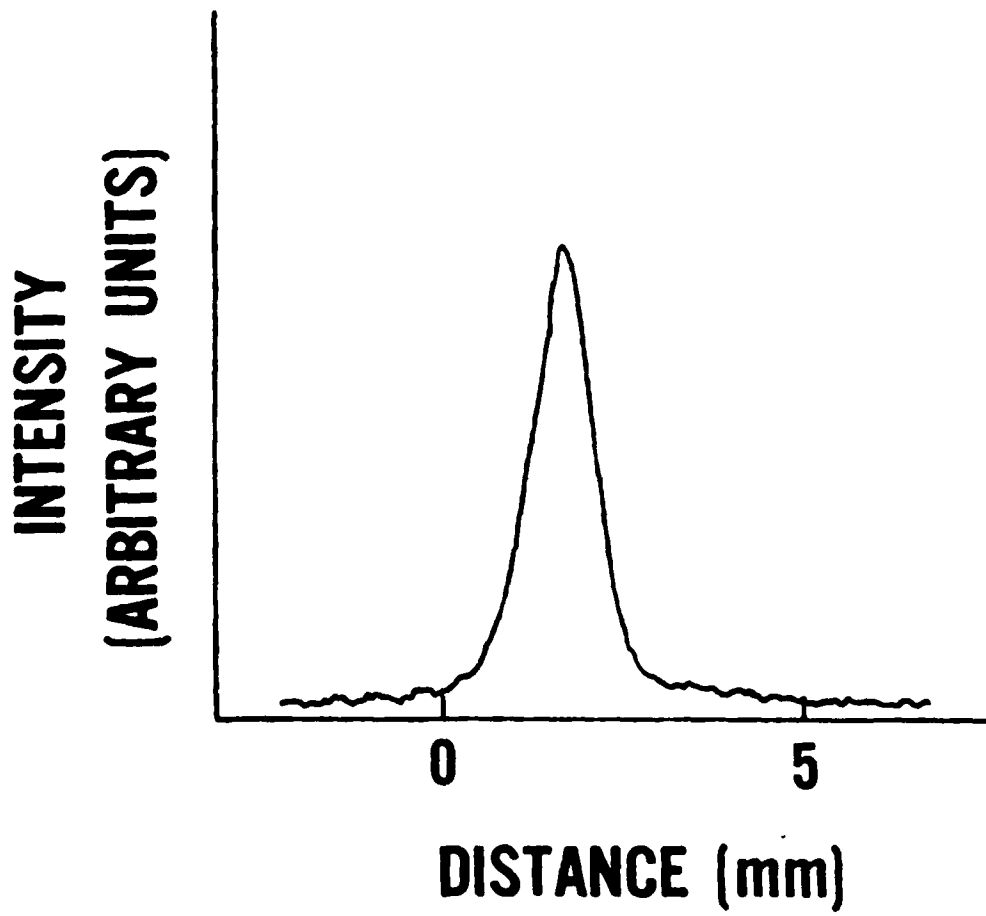


FIGURE 3.

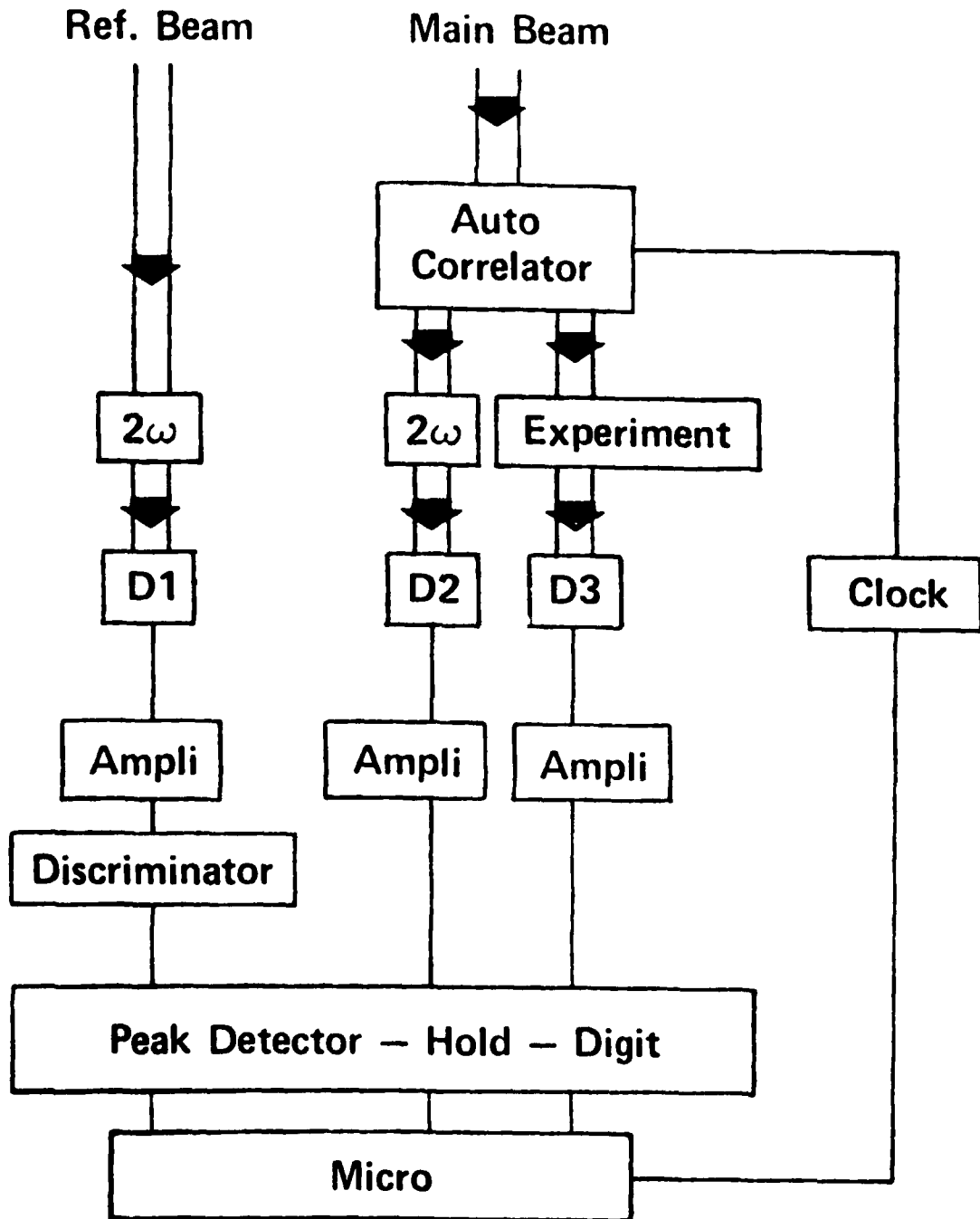
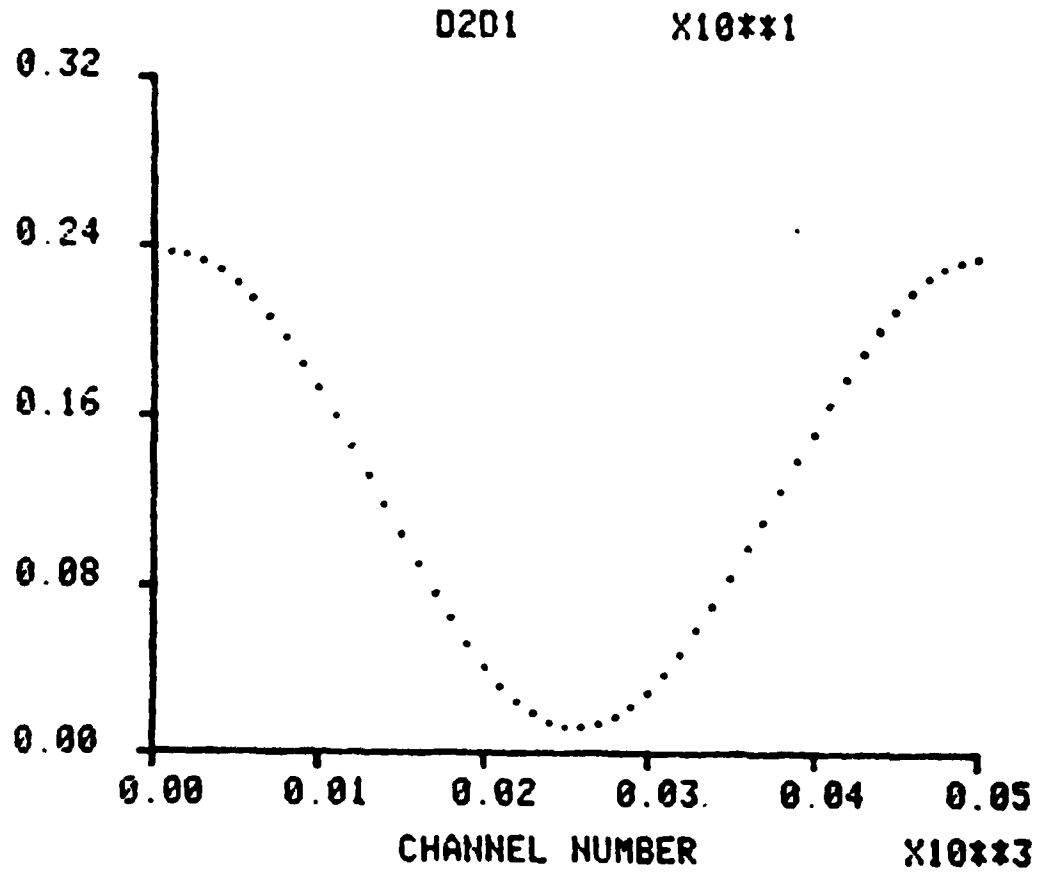


FIGURE 4.



TIME AT START OF GROUP = 0.0000 SECONDS  
TRAVEL AT START OF GROUP = 0.0000 MICRONS

FIGURE 5a.

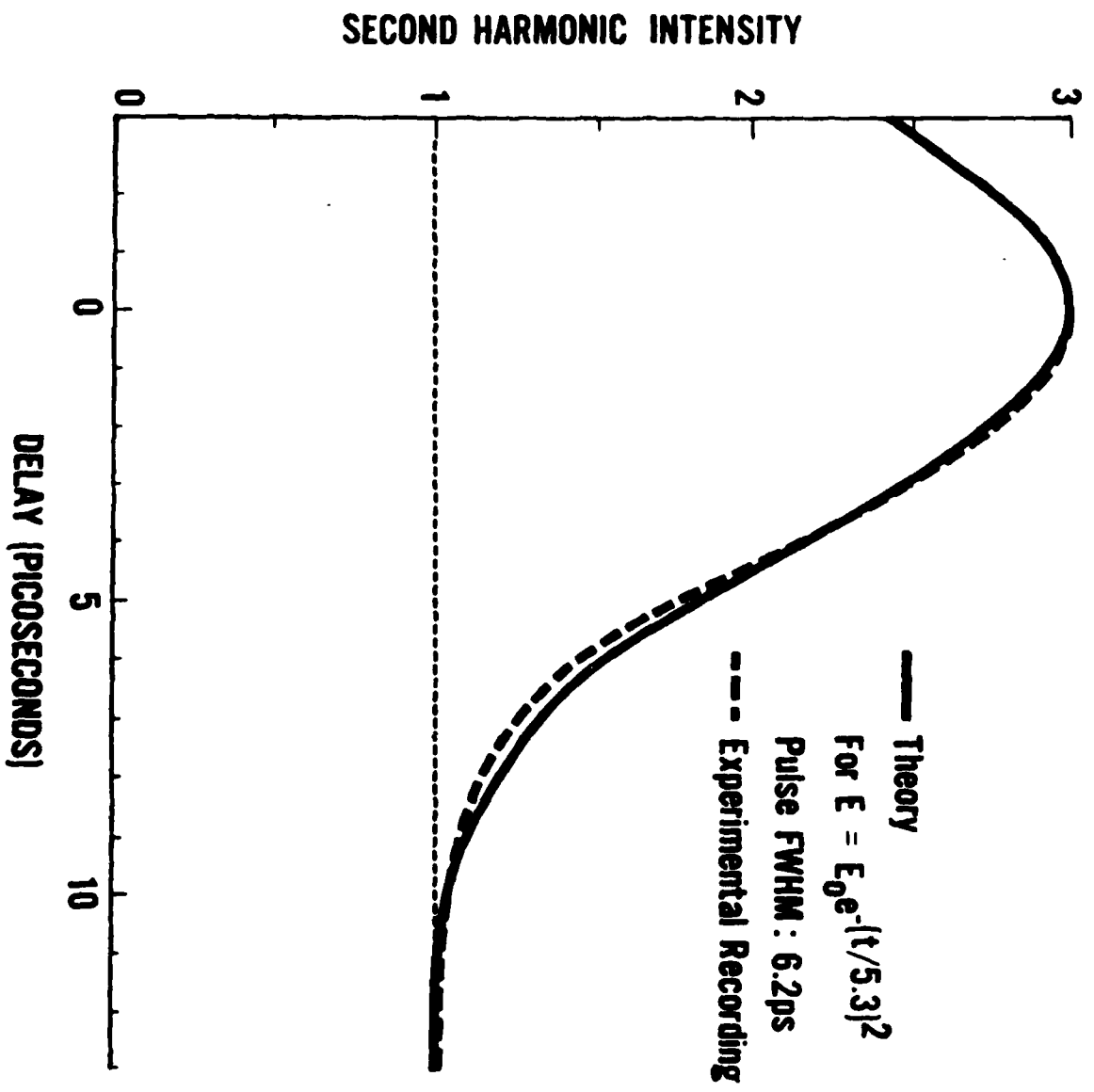
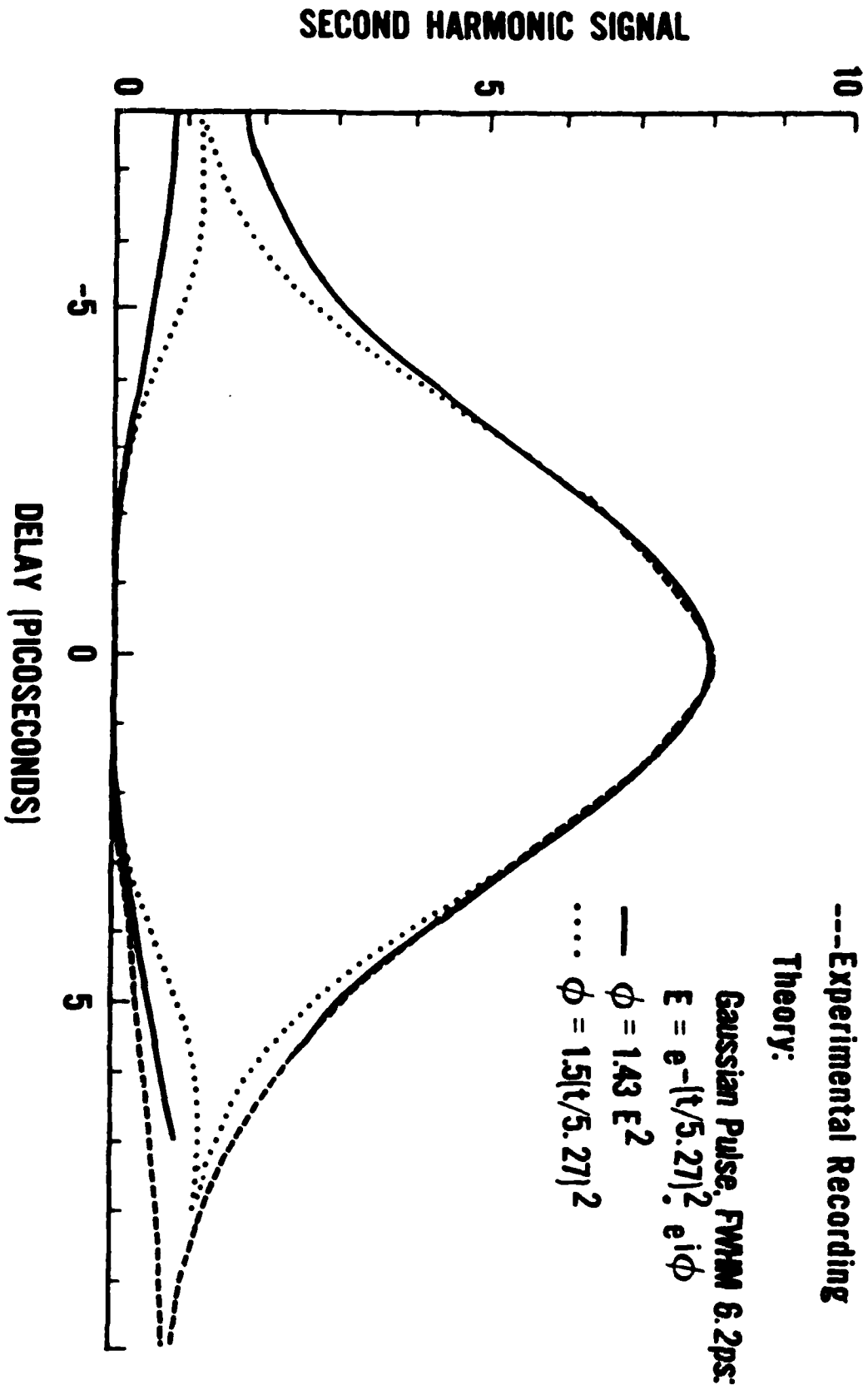


FIGURE 5b.

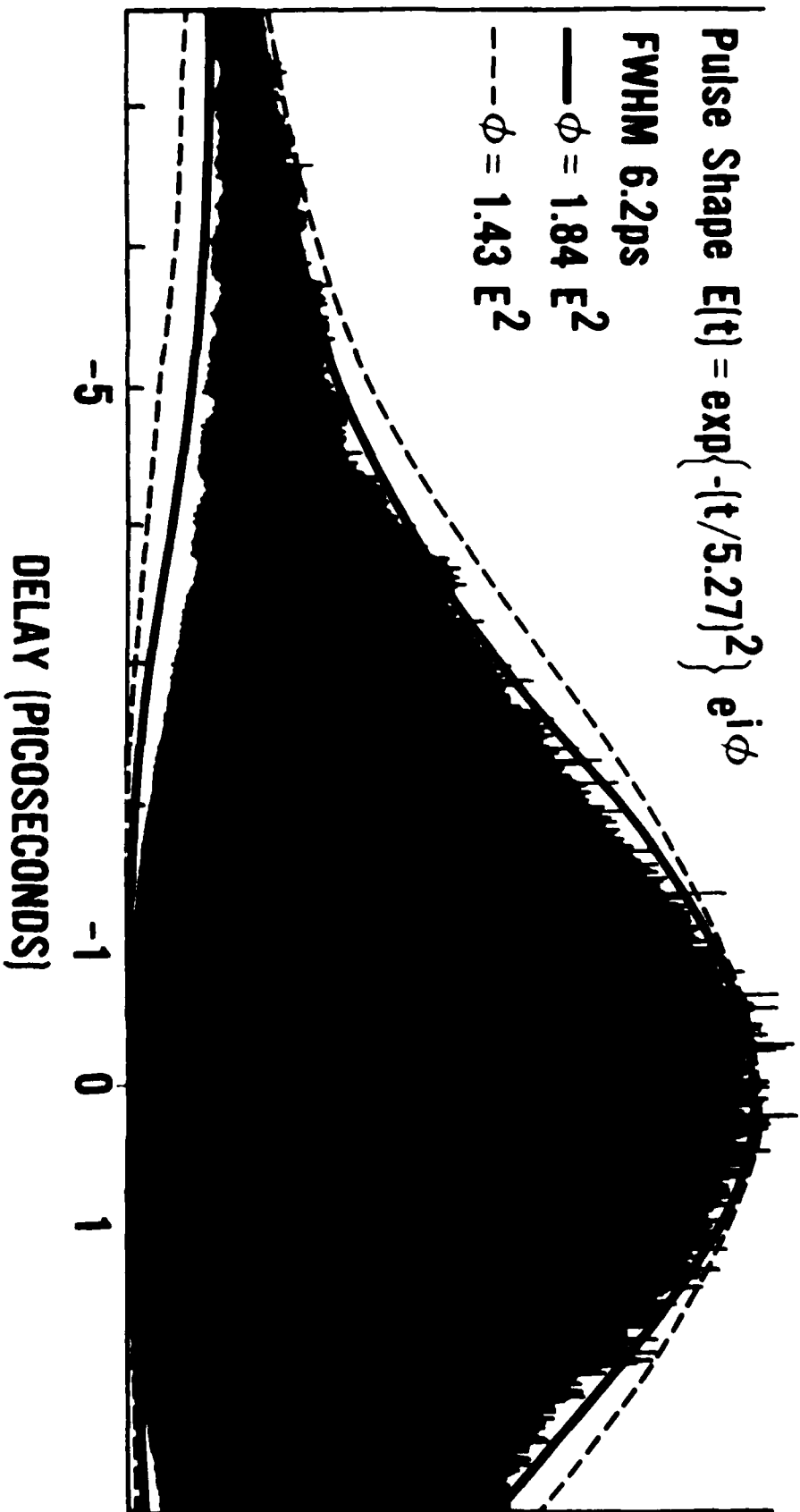


Pulse Shape  $E(t) = \exp\left\{-\left(t/5.27\right)^2\right\} e^{i\phi}$

FWHM 6.2ps

—  $\phi = 1.84 E^2$

---  $\phi = 1.43 E^2$



A P P E N D I X B

**MULTIPHOTON IONIZATION UNDER SEQUENTIAL EXCITATION  
BY COHERENT PULSES**

J.-C. Diels  
Center for Applied Quantum Electronics  
Department of Physics  
North Texas State University  
Denton, Texas 76203

and

J. Stone  
Center for Laser Studies  
University of Southern California  
Los Angeles, CA 90089-1112

**Abstract**

The use of pulse sequences offers a solution to the conflicting requirements of spectral selectivity and high peak intensities needed to study multiphoton processes. In addition, it is shown that random--rather than regular--pulse sequences can provide unique information on the influence of coherence on a resonant multiphoton process, because the coherence can be adjusted independently of the resonance condition.

## I. INTRODUCTION

Attention has been drawn in recent years to the possible use of pulse sequences to enhance quantum beat phenomena in molecules,<sup>1</sup> or to selectively enhance weak spectral lines.<sup>2</sup> Phase shifts in the light field for a single pair of pulses can be used to distinguish between single and multiphoton processes.<sup>3</sup> Statistically distributed phase switching on a CW field can give it the spectral and driving characteristics of a line broadened source.<sup>4</sup> Here we discuss an application of pulse sequences in the area of laser driven reactions. We choose as an example multiphoton ionization of atoms. However, the approach used here applies also to multiphoton dissociation of molecules--which has been the subject of extensive theoretical investigation<sup>5</sup>--or to any other process dependent on the absorption of several photons.

Two types of sequential excitation will be considered: deterministic or statistical. The motivation for using a sequence of identical pulses with a well defined phase relationship, is to combine the spectral selectivity offered by a regular pulse train, with the high peak intensities of picosecond pulses, which are needed to excite higher order processes.

A dimension of nonlinear mechanisms that is subject to experimental test is the coherence or lack of coherence in the process. But, as we discuss below, the single pulse experiments that have been the mainstay of this area provide a fairly limited test of coherence. Multimode versus single mode operation has been used<sup>6,7</sup> to vary the "coherence" of the laser source. This procedure has the disadvantage of varying the bandwidth--hence the resonance condition--simultaneously with the pulse coherence. We will show how a sequence of pulses of controlled phase can be used to vary the source coherence without affecting its central frequency or its spectral width.

By choosing the delays and phase between pulses to fit a chosen statistical distribution, we can study how a multiphoton process is affected by that statistics. Such an approach, of averaging many measurements with a predetermined setting of delays and phases (to fit a given photon statistics), will be shown to have several advantages over other methods of studying the influence of source coherence on a multiphoton resonant process. As an illustrative example for the latter, we have chosen multiphoton ionization in a metal vapor, in presence of a two photon resonance.

## II. THEORETICAL MODEL

We consider an atomic system in conditions of two photon resonance with electromagnetic radiation at  $\omega$ , which can be ionized with a single photon transition from the upper state (Fig. 1). The evolution equations for the components of the density matrix for an exciting electric field of slowly varying amplitude  $\mathcal{E}$ , can be written (1):

$$i\dot{\sigma}_{12} = - (i\Delta\omega + \frac{1}{T_R} + \frac{\gamma_2}{2}) i\sigma_{12} - (\sigma_{22} - \sigma_{11}) \mathcal{E}^2 \quad 1$$

$$\dot{\sigma}_{22} - \dot{\sigma}_{11} = 4 \operatorname{Re} \{ \mathcal{E}^{*2} (i\sigma_{12}) \} - \gamma_2 \sigma_{22} \quad 2$$

$$\dot{\sigma}_{11} + \dot{\sigma}_{22} = - \gamma_2 \sigma_{22} \quad 3$$

$T_2$  is the phase relaxation time,  $\gamma_2 = 2\gamma\mathcal{E}^2$  the photoionization rate from the upper level 2,  $\Delta\omega = 2\omega - \omega_{12} - \delta\omega_{21}$  is the frequency detuning from resonance, including the Stark shift  $\delta\omega_{12} = \alpha\mathcal{E}^2$ . With the substitution  $i\sigma_{12} = Q$ ,  $(\sigma_{22} - \sigma_{11})/2 = W$ , and  $E^2 = 2\mathcal{E}^2$ , and neglecting relaxation and ionization, the equations can be rewritten:

$$\dot{Q} = -i\Delta\omega Q - W E^2 \quad 4$$

$$\dot{W} = \operatorname{Re}(E^{2*} Q) \quad 5$$

with the initial condition  $W(t=0) = -1$ .

The equation (4) can be formally integrated, yielding

$$Qe^{i\Delta\omega t} = - \int_{-\infty}^t W E^2 e^{i\Delta\omega t'} dt' \quad 6$$

After a pulse has passed,  $Q(t \gg \tau) = E_{2F}(\Omega)$ , where  $E_{2F}(\Omega)$  is the Fourier transform of  $E^2(t)$ . From the conservation relation  $|Q|^2 + W^2 = 1$ ;

$$|Q|^2 = 1 - W^2 = -2W_0 \Delta W = 2\Delta W, \quad 7$$

where  $\Delta W = W(t = \infty) - W(t = 0)$ . Combining Eqs. (6) and (7), gives the energy absorbed by the two-level system:

$$2\Delta W = - |E_{2F}(\Delta\omega)|^2 \quad 8$$

The number of ions produced is simply the number of "lost atoms"  $1 - \sigma_{22}(t = \infty) - \sigma_{11}(t = \infty)$  in the system of equations (1)-(3). The number of ions can also be estimated by integrating the ionization rate:

$$N_{\text{ions}} = \int \gamma |E|^2 \sigma_{22} dt \quad 9$$

For small population transfers,  $\sigma_{22} = \Delta W$ , and

$$N_{\text{ions}} = \int \gamma |E|^2 \Delta W(t) dt \quad 10$$

Replacing  $\Delta W$  by its average value  $W(\infty)/2$ :

$$N_{\text{ions}} = \frac{\gamma}{4} |E_{2F}(\Delta\omega)|^2 \times \theta \quad 11$$

where  $\theta = \int_{-\infty}^{\infty} |E|^2 dt$  is the "pulse area" or tipping angle of the pseudopolarization vector in the vector model of the two-photon resonant interaction (2,3).

The expressions above hold in the approximation of weak excitation ( $\theta$  small), no Stark shift (or any Stark shift but square pulse excitation). We see that both the absorption and the photoionization reflect the excitation spectrum. The photoionization spectrum is simply a fraction (proportional to the "pulse area") of the Fourier spectrum of the Rabi frequency (which is, in this case, proportional to the square of the exciting electric field).

### III. COHERENCE AND SPECTRAL CHARACTERISTICS

We will consider now more specifically the spectral characteristics (i.e., number of ions versus frequency) of an excitation mode of a sequence of pulses. In general, even if each individual pulse is pure in frequency (real amplitude function) the sequence of various pulses will be represented by a complex function  $E$  (because of the relative phase between pulses). A general property of the system of equations (4,5) is that  $W$ --which determines in first approximation the photoionization remains unchanged under a transformation  $E \rightarrow E^*$ ,  $\Delta\omega \rightarrow -\Delta\omega$  (indeed, under this transformation, Eq. 4 is transformed in its complex conjugate and Eq. 5 remains unchanged). This symmetry implies that the photoionization spectrum of a single unchirped pulse to ( $E$  real) is symmetric. The symmetry is broken however in the case of a sequence of pulses with a phase difference  $\Delta\phi$  different from 0 or  $\pi$ , for which we no longer have  $E = E^*$ .

It was shown in the preceding section that at least part of the response of the medium may be inherent in a Fourier decomposition of the pulse sequence. Since we will be considering sequences of pulses that are identical except for their relative phases and delays, the overall time dependence of the signal can be written as:

$$F(t) = \sum_{n=1}^N e^{2i\phi_n} f(t + \tau_n) \quad 12$$

In Eq. (12)  $F(t)$  denotes the generalized (complex) Rabi frequency driving the system of equation 4,5, and  $f(t)$  is the Rabi frequency ( $E^2$ ) for each individual pulses. The  $n^{\text{th}}$  pulse is centered at  $\tau_n$ , and  $\phi_n$  is its absolute phase. The spectrum of  $F(t)$  is the function:

$$F(\Omega) = f(\Omega) g(\Omega) \quad 13$$

which is equal to the spectrum of a single pulse  $f(\Omega)$  "modulated" by the function  $g(\Omega)$  given by

$$|g(\Omega)| = \sum_{n=1}^N e^{2i\phi_n - i\Omega\tau_n} \quad 14$$

A particular case of interest is the coherent sequence of  $N$  identical pulses with relative time delay  $\Delta\tau$  and (relative) dephasing  $\Delta\phi$  ( $\phi_n = n\Delta\phi$ ;  $\tau_n = n\tau$ ), which leads to the particularly simple form for  $g(\Omega)$ :

$$g(\Omega) = \frac{\sin\left(N\Delta\phi - \frac{\Omega\Delta\tau}{2}\right)}{\sin\left(\Delta\phi - \frac{\Omega\Delta\tau}{2}\right)} \quad 15$$

The spectral intensity  $|g(\Omega)|^2$ , which was shown to be in a limiting case proportional to the ionization spectrum, is illustrated in Fig. 2 for a  $N=10$  pulse sequence. The multiphoton ionization from exactly this type of pulse sequence will be considered in the following section.

#### IV. IONIZATION BY A REGULAR PULSE SEQUENCE

We consider now the multiphoton ionization produced by a sequence of identical pulses, regularly spaced in phase and time. The system of equations (1-3) is solved numerically for the four initial conditions corresponding to each of the elements of the density matrix set successively equal to 1. The matrix formed by the four sets of solutions forms an operator which, multiplied by any set of initial conditions, will give the density matrix as transformed by one pulse. Between pulses, the components of the density matrix relax according to the resonance condition and the relaxation times. The phase of each successive pulse is taken into account by a simple transformation (rotation) of the operator matrix. The value taken by  $1 - \sigma_{11} - \sigma_{22}$  after passages of the pulses is the fraction ionized.

Fig. 3 shows the ionization spectrum for a series of 10 square pulses of area 1, separated by 100 psec. The pulse duration is 10 psec. The two spectra correspond to a phase difference between pulses of  $-0.5\pi$  (—) or  $-.1\pi$  (----). Even though the condition  $\theta \ll 1$  does clearly not apply for the pulse

trains, and not even for the individual pulses, the spectrum qualitatively resembles that of the excitation pulses. In fact, the photoionization curves show all the characteristic features of a Fourier spectrum: the overall width is related to  $1/\tau$ , an increase of the phase difference between pulses shifts correspondingly the photoionization spectrum, and the width of the individual peaks in the photoionization spectrum decreases with increasing delay between pulses.

The Stark shift introduces an additional complexity, by essentially creating a different resonance condition during and between pulses. This effect is demonstrated by the simple example of a sequence of two square pulses shown in Fig. 4. Increments of delay between the pulses by multiples of  $(2\pi)/(\text{Stark shift})$ , produce the same number of ions at resonance and at a detuning from resonance equal to the Stark shift. Departure from the simple approximations (6-10) will be particularly significant for large area pulses. "Photoionization spectroscopy" with a sequence of large area pulses will enable a direct measurement of the photoionization rate from the upper state through the width of the individual peaks. Indeed, as shown in Fig. 5, the width of each peak in the photoionization spectrum is seen to increase with the transition rate to the continuum. It is interesting to note (Fig. 5) that the peak ionization is smaller for the higher ionization rate. The reduction in peak ionization rate is due to the increased dephasing associated with the transition rate to the continuum, resulting in a decrease in coherent excitation of the upper level.

## V. IONIZATION BY A RANDOM PULSE SEQUENCE

An incoherent field can be described by a density matrix corresponding to an incoherent superposition of coherent states.<sup>8</sup> We choose to use for this superposition a series of identical pulses with a random distribution of delays and phases.

Under certain conditions, a large number of experiments performed with a few pulses, for which the relative delays are distributed according--for instance--to a Poisson Statistics, will have the same average result as the same experiment performed once with a very large number of pulses, distributed according to the same statistics. The average time between pulses has to be shorter than the coherence time of the particular resonance under investigation. We demonstrate next that, if the pulses are randomly distributed, the time evolution of the system driven by a sequence of identical pulses is proportional to the number of pulses, and to the total fluence delivered, as expected for incoherent excitation. If, instead, the pulses are applied in phase and, for instance, in condition of two photon resonance, the absorption by the system is proportional to the square of the number of pulses. For demonstration purposes, let us consider near two-photon resonance ( $E^2 \gg \Delta\omega$ ) and weak pulses such that the approximation  $W = W_0$  can be made in Eq. 4. Each of the pulses of "area

$$\Delta\theta = \int_{t_i}^{t_f} E^2 dt \text{ produces an increase in polarization}$$

$$Q = W_0 \Delta\theta \exp(i\phi) \quad 16$$

If the pulses are all in phase (pulses equally spaced and in phase),  $\Delta\theta$  is a constant angle, and after  $N$  pulses,  $Q = N\Delta\theta$  and the energy absorbed  $W$  is proportional to the square of the number of pulses:

$$W = \frac{N^2 \Delta\theta^2}{2} \quad 17$$

If the distribution of pulse delays is random ( $\Delta\omega\tau_d \gg 1$ ), then the phase in Eq. 1 is a random variable, and the vector  $Q$  makes a random walk of  $N$  steps  $\Delta\theta$  in the complex plane, starting from the origin. The resultant polarization is  $Q = N\Delta\theta$ , and the energy absorbed is proportional to the number of pulses:

$$W = N \frac{\Delta\theta^2}{2} \quad 18$$

It should be noted that by using a sequence of pulses, we can compare coherent (as in Eq. 17) versus incoherent (as in Eq. 18) excitation, under the same conditions of total fluence and peak intensity. As expected, it is only in the case of incoherent excitation that the evolution of the system can be simply proportional to the total fluence delivered. The intensity dependence of the multiphoton process is not invoked in comparing the incoherent versus coherent case. The above considerations still hold in the more general case of a  $n$ -photon transition. The only difference is a generalized Rabi frequency in  $E^n$ . Equations 16 through 18 remain unchanged, with  $\Delta 0 = \int_{t_i}^{t_f} E^n dt$ . In the approximation  $E^n \gg \Delta\omega$ , and no intermediate level resonance, coherent excitation is characterized by an absorbed energy proportional to the square of the number of pulses, while the absorption is directly proportional to the number of pulses in the incoherent case.

In order to study the influence of source coherence on the photoionization spectrum of lithium, we calculated the number of ions as a function of pulse wavelength for a coherent and an incoherent sequence of 10 pulses (Fig. 6). The "incoherent" curve (solid line, Fig. 6) corresponds to an average of 500 pulse sequences, each with a different set of relative delays taken from a Poisson distribution. The relative phases are uniform random numbers between 0 and  $2\pi$ . The total area in each sequence of pulses is 1. As can be seen from Fig. 6, the photoionization from a coherent sequence (10 pulses equally spaced, relative phase  $\pi/2$ , dashed line in Fig. 6) can be much larger than that of the incoherent excitation. This result may appear to be in contradiction with experimental results of Lecompte, et al. [6], on the influence of coherence on multiphoton excitation. In the case of nonresonant  $N$  photon ionization of atoms reported in ref 6, the ionization probability is proportional to the  $N$ th power of the laser intensity, and therefore very sensitive to the transient intensity peaks that

occur in a multimode laser pulse. The dependence of multiphoton ionization on laser coherence was studied by varying the number of oscillating laser cavity modes between one and one hundred. It has been estimated [9] that, in that case, a 20 mode laser is a good approximation of an incoherent source. The situation is more complex in the case of resonant multiphoton ionization as we are considering here. Indeed, the number of oscillating modes is varied by changing the bandwidth of the cavity. Therefore, the parameter "coherence" cannot be controlled independently of the resonance condition, since the spectral width of the laser source increases with decreasing coherence. In the approach used here however, the laser coherence is modified at constant bandwidth, since the spectrum of the pulse sequence is contained within the spectrum of a single pulse.

It is interesting to note that, in a recent experimental study of 4 photon (3 photon resonant) ionization of caesium atoms, Lompre, et al. [7] found also an increase in the width of the spectral dependence of the ionization, for incoherent versus coherent excitation. The hyperfine structure of the resonance is still observed in coherent excitation, while it is not in the incoherent case (ref. 7, Fig. 8). However, in that particular experiment [7], the coherence was varied by changing the number of modes of the laser, and comparing data for the same average intensity. Therefore, temporal fluctuations make the peak intensity highest in the incoherent case, resulting in a higher ionization in the incoherent case than in the coherent case. In an experiment in which the coherence is varied by varying the temporal distribution of identical pulses, as suggested here, the peak intensity as well as the spectral bandwidth remain constant, while the coherence is modified within the pulse spectrum.

## Photon Statistics

Let us consider a limiting case where each pulse of the sequence contains only one photon. The "pulse sequence statistics" is then nothing else than the photon statistics of the radiation field. The number of pulses  $N$  is now the number of photons in the excitation, each of these photon  $\hbar\omega$  driving coherently a  $n$ -photon resonant system (i.e., a two level system of energy  $n\hbar\omega$ ). For instance, in the simple argument at the beginning of this section, the elementary increment of the  $n$ -photon off diagonal element becomes

$$\Delta\theta = \int_{t_i}^{t_f} E^n dt = [\hbar\omega]^{n/2} \quad 19$$

$n$  being a proportionality coefficient.

It should be noted that the photon energy does not appear explicitly in any calculations carried out in the slowly varying envelope approximation (SVEA). The statistical sequence of identical macroscopic coherent pulses (each of them being a coherent superposition of  $M$  photons) interacting with the  $n$ -photon resonant atoms, is identical (within the SVEA) to a photon statistics in a fictitious world where Planck's constant is  $M\hbar$ . The transition frequency at  $\omega_0 = n\omega$  is in condition of  $n$ -photon resonance with each pulse  $(M\hbar)\omega_0 = n(M\hbar)\omega$ . Since Planck's constant appears only implicitly (in the scaling of the generalized Rabi frequency  $E$ ) in the theoretical model, all the equations of the theoretical model remain unchanged by the "transformation." The elementary increment of the off diagonal element for the standard pulse of the train can also be expressed in terms of the "pseudo photon" energy  $(M\hbar)\omega$ , in a similar way as in Eq. 19:

$$\Delta\theta = \int E^n dt = n[(M\hbar)\omega]^{n/2} \quad 20$$

This similitude offers an intuitive justification to the use of a pulse sequence to study the statistical response of a multiphoton resonant system. We are

essentially creating a pseudo photon statistics. This concept is legitimized because Planck's constant does not appear explicitly in this formalism (i.e., the photon energy is still small compared with the total excitation energy). Since the model of the pseudostatistics concept is equivalent to the theoretical model used in section III, it does not bring any new light to the problem. However, it offers a convenient interpretation to the approach that is being taken here, to study coherence effects through the use of pulse sequences.

The work was supported by the Air Force Office of Scientific Research (AFOSR) under Grant No. 820332, and by the Robert A. Welch Foundation.

## REFERENCES

1. A. Villaeys and K. F. Freed, Chem. Phys. 13, 271 (1976).
2. W. S. Warren, D. P. Weitekamp, and A. Pines, J. Chem. Phys. 73, 2084 (1980); W. S. Warren and A. H. Zewail, J. Chem. Phys. 78, 2279, 2298 (1983).
3. J.-C. Diels, J. Stone, S. Besnainou, M. F. Goodman, and E. Thiele, Opt. Comm. 37, 11 (1981).
4. M. F. Goodman, J. Stone, and E. Thiele, J. Chem. Phys. 63, 2929 (1975).
5. J. Stone and M. F. Goodman, J. Chem. Phys. 71, 408 (1979) and references contained therein.
6. C. Lecompte, G. Mainfray, C. Manus, and F. Sanchez, "Laser temporal-coherence effects on multiphoton ionization processes," Physical Review A, Vol II, pp. 1009-1015 (1975).
7. L.-A. Lompre, G. Mainfray, C. Manus and J. P. Marinier, "Laser light statistics and bandwidth effects in resonant multiphoton ionization of caesium atoms at 1.059  $\mu\text{m}$ ", J. Phys. B: At. Mol. Phys., Vol 14, pp. 4307-4326 (1981).
8. Glauber, Phys. Rev. 131, 2766 (1963).
9. J.-L. De Bethune, Nuovo Cimento B 12, 101 (1972).

## FIGURE CAPTIONS

Figure 1. Level diagram.

Figure 2. Plot of the spectral intensity for a sequence of 10 identical square pulses, as defined in Eq. 15.

Figure 3. Ionization versus angular frequency ( $\text{ns}^{-1}$ ) for a sequence of 10 Gaussian pulses, with an interpulse separation of 0.1 ns. The area (energy) of each individual pulse is 1, and their duration (FWHM of the intensity) is 0.01 ns. Two different cases of relative phase difference are shown:  $\Delta\phi = -\pi/2$  (—) and  $\Delta\phi = -0.1$  (-----). The parameters are taken from the 2s-4s transition of lithium (Stark shifts  $-1.5 E^2$ ; ionization rate from the 4s level:  $0.07 E^2$ ).

Figure 4. Ionization versus angular frequency ( $\text{ns}^{-1}$ ) for a sequence of two square pulses. The individual pulses have a duration of 0.05 ns and an amplitude of  $E = 10 \text{ ns}^{-1/2}$ . The medium parameter are the same as for Fig. 2 (hence the Stark shift is  $-150 \text{ ns}^{-1}$ ). The solid line shows the ionization spectrum for a sequence of two pulses  $90^\circ$  out of phase following each other without delay. For the dashed line, the two successive pulses,  $90^\circ$  out of phase, are separated by a delay of  $[2 / (\text{Stark shift})]$ .

Figure 5. Single peak of the ionization spectrum (% ions versus angular frequency in  $\text{ns}^{-1}$ ), for two different ionization rates. The exciting field consists in a sequence of 10 Gaussian pulses, of 0.01 ns duration (FWHM), and area  $\theta = \int E^2 dt = 3$ . The successive pulses are 0.4 out of phase. The medium parameters are the same as in the preceding figures, except for the ionization rates  $\gamma E^2$  being considered here. The scale to the right corresponds to the ionization rate of  $0.07 E^2$ .

(-----) while the scale to the left pertains to the higher ionization rate of  $0.44 E^2$  (——).

Figure 6. Ionization versus angular frequency ( $\text{ns}^{-1}$ ) for a sequence of 10 pulses. Each pulse is Gaussian shaped of area 0.1. The solid line corresponds to a random pulse sequence; the dashed line to a sequence of equally spaced (0.09 ns) pulses, each  $90^\circ$  out of phase with the former. Each pulse of the sequence is Gaussian, with a duration of 0.01 ns (FWHM). The statistical result (——) is obtained by taking the average of 500 "excitations," each with a sequence of pulses distributed (in relative delay) according to a Poisson distribution. The relative phases between pulses are taken to be random numbers between 0 and  $2\pi$ . The medium parameters are the same as for Fig. 2. The average delay between pulses is 0.09.

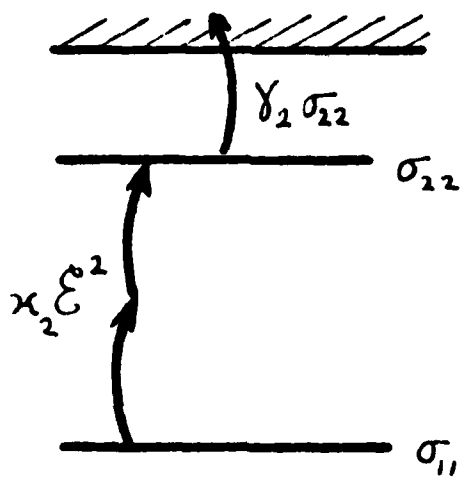


Figure 1.

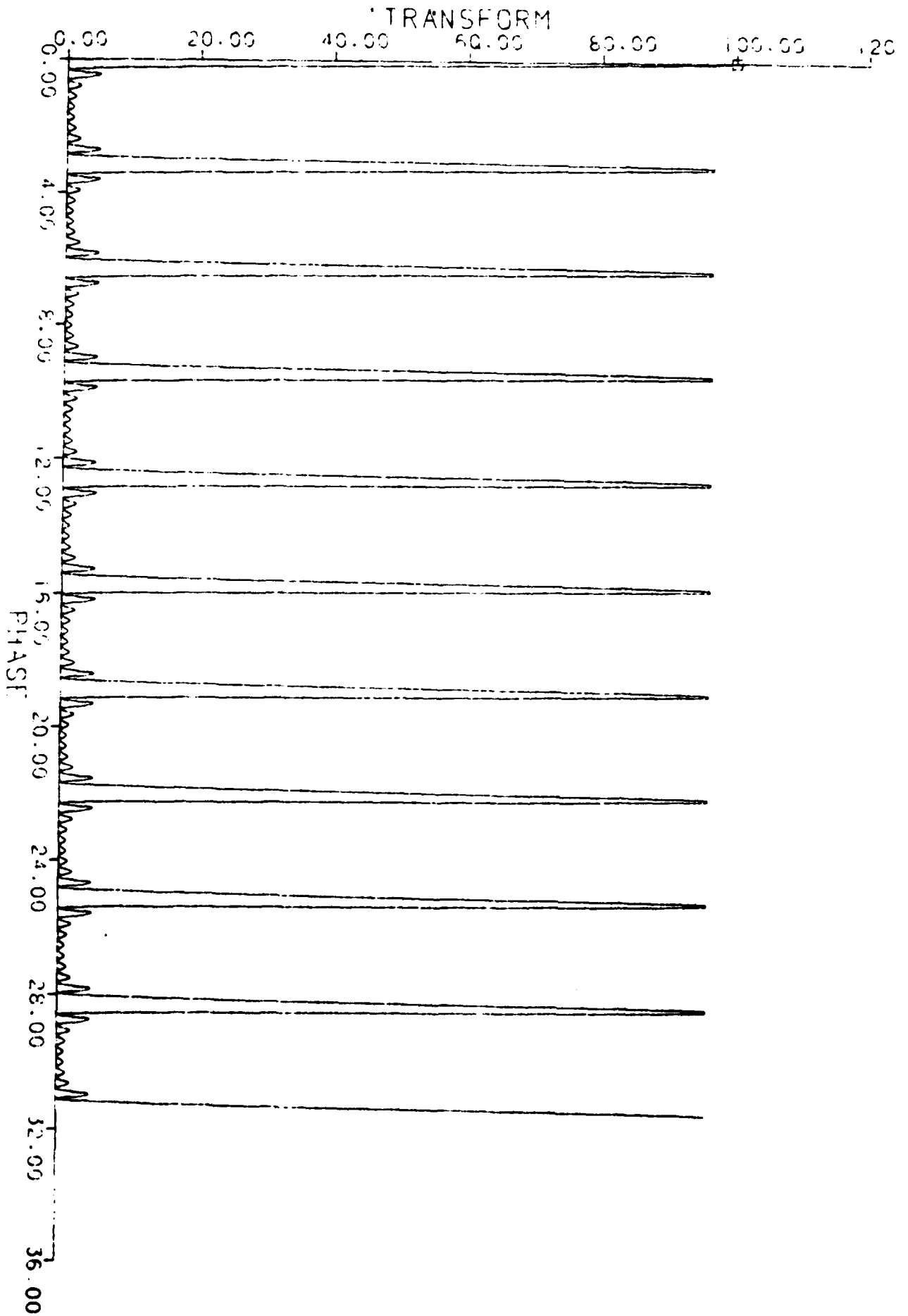


Figure 2.

# IONIZATION FOR A 10 PULSE SEQUENCE

PULSE DURATION: 0.01 nsec

PULSE "AREA": 1

RELATIVE DELAY:  $T_D = 0.1$  nsec

— PHASE DIFFERENCE BETWEEN PULSES:  $-\frac{\pi}{2}$

----- PHASE DIFFERENCE BETWEEN PULSES:  $-0.1\pi$

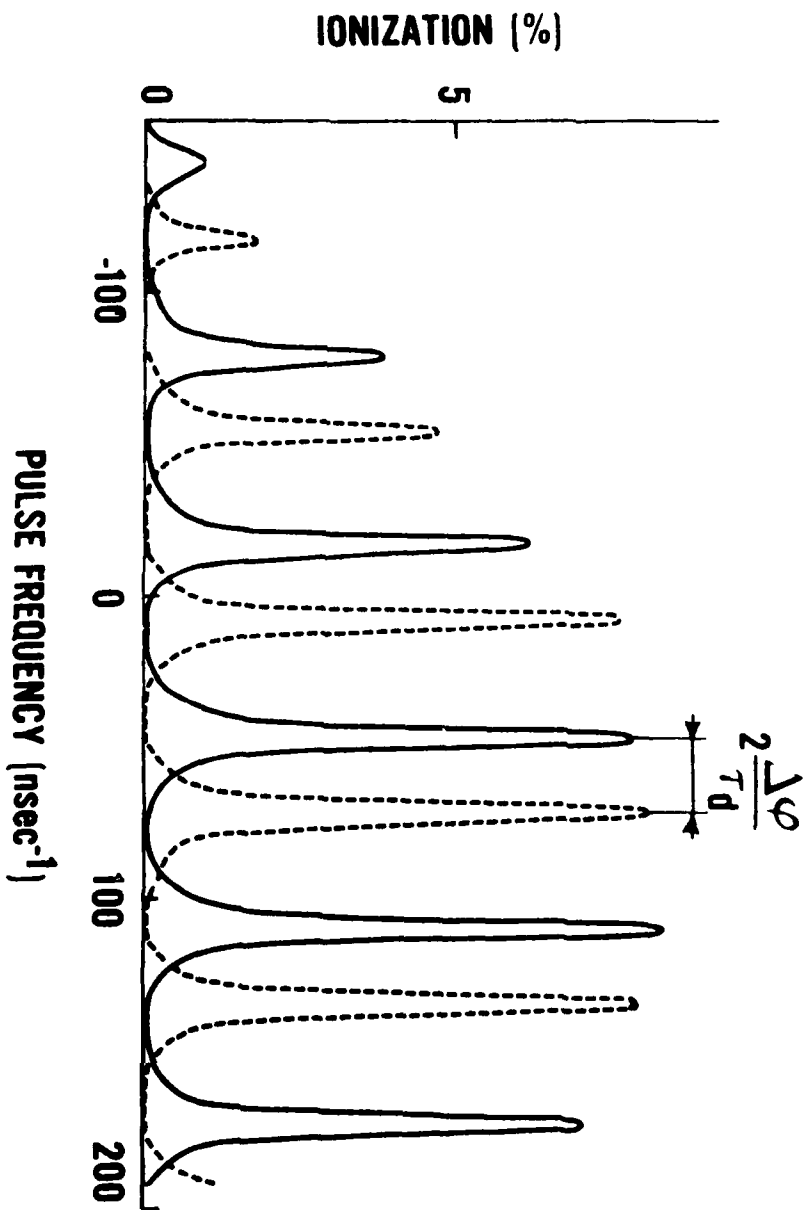


Figure 3.

# IONIZATION FOR A 2 PULSE SEQUENCE

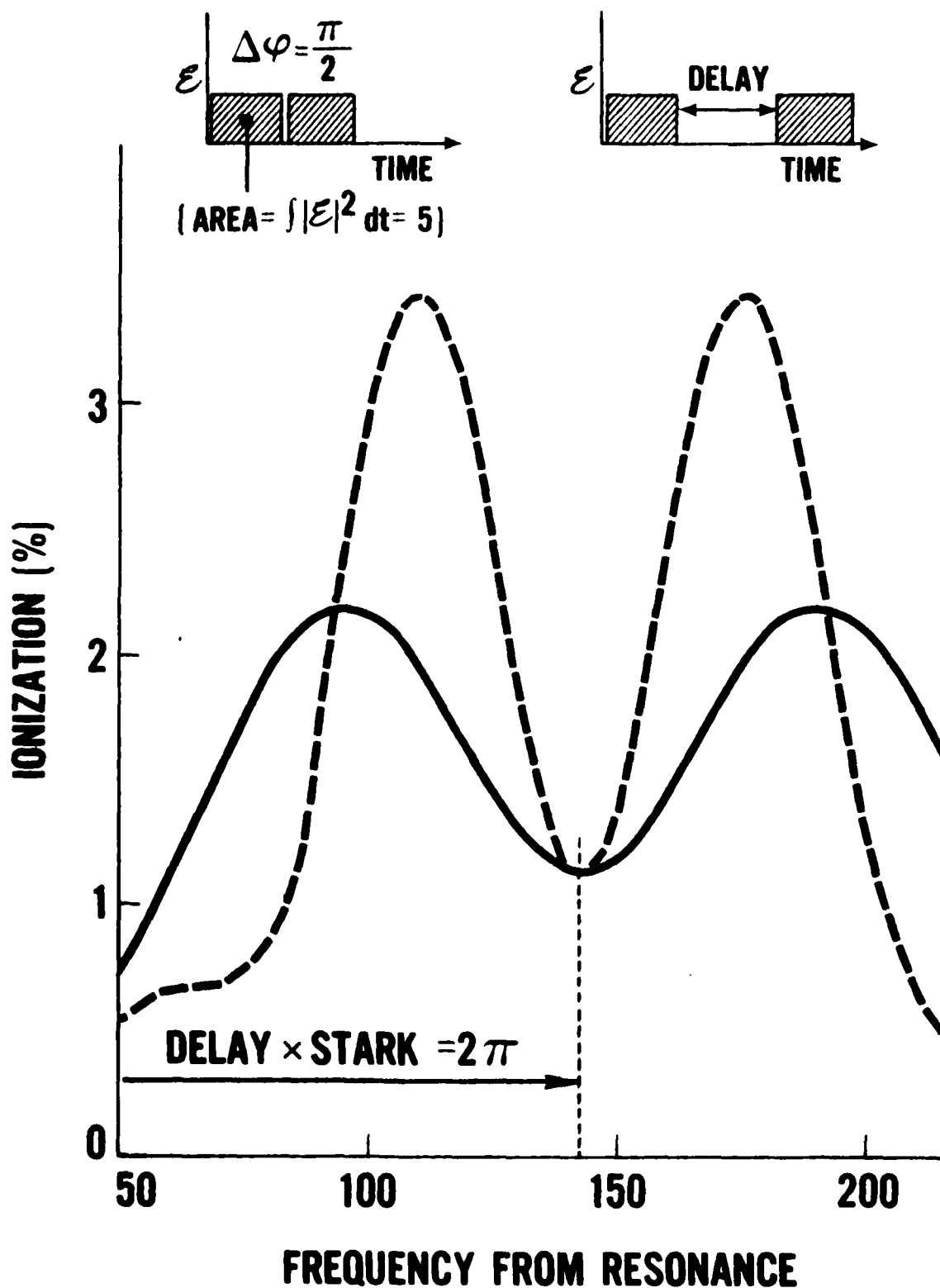


Figure 4.

# IONIZATION FOR A 10 PULSE SEQUENCE

PULSE "AREA":3

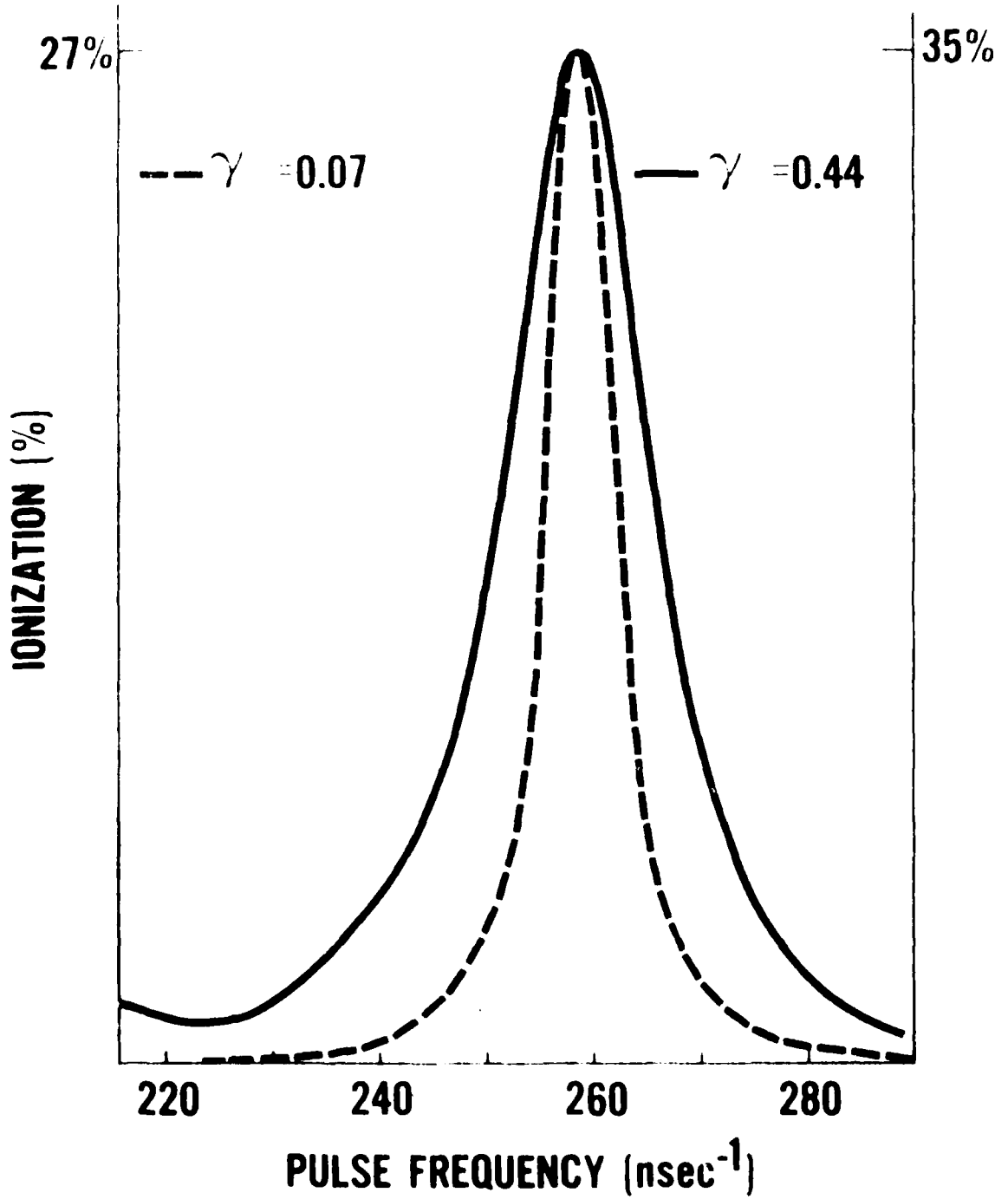


Figure 8.

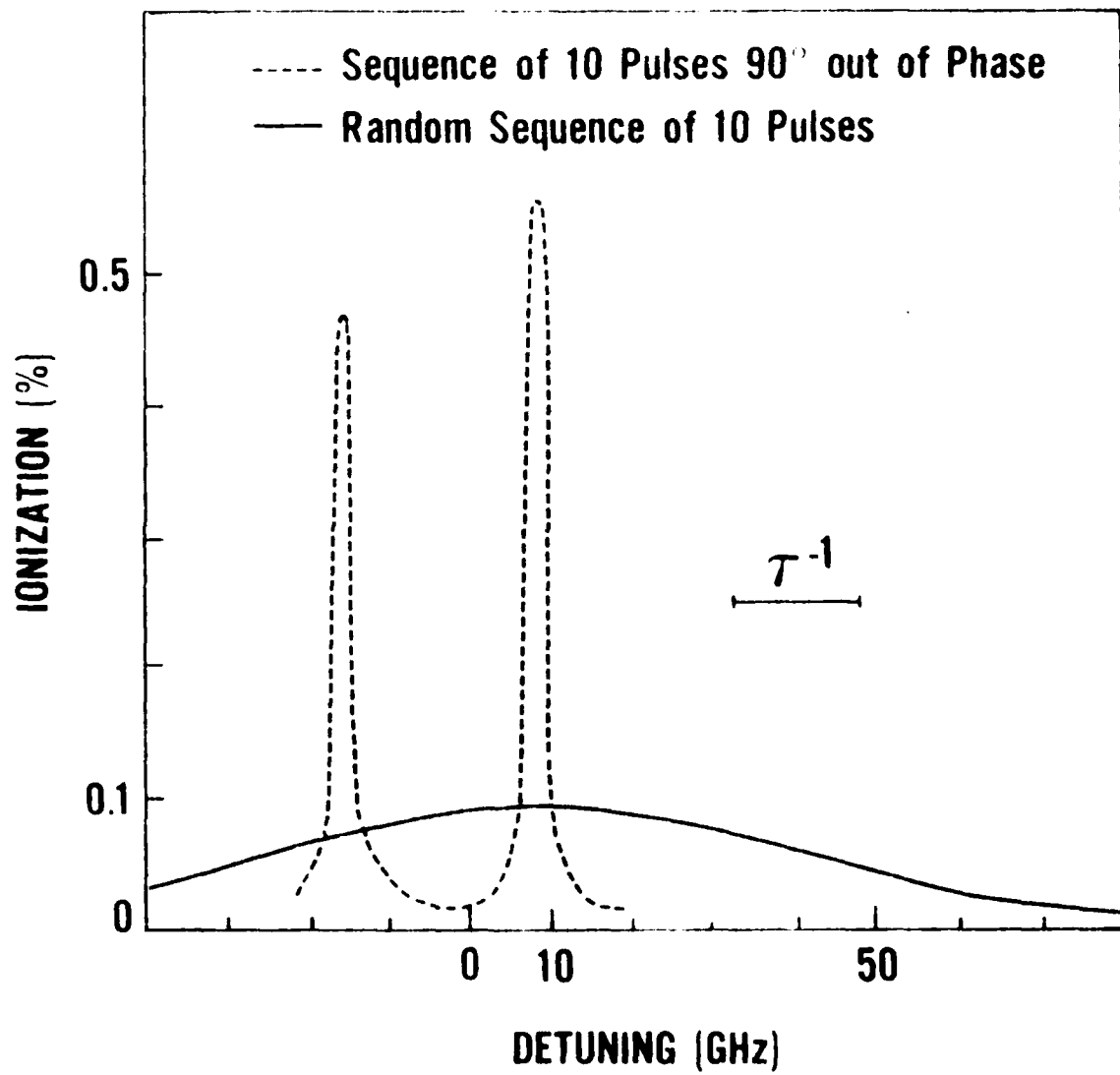


Figure 1

A P P E N D I X C

INTERFEROMETRIC AUTOCORRELATIONS APPLIED TO THE STUDY OF  
MULTIPHOTON COHERENCE

H. Vanherzeele and J.-C. Diels  
Center for Applied Quantum Electronics  
Department of Physics  
North Texas State University  
P.O. Box 5368; NT Station  
Denton, Texas 76203  
817-565-3308

A new method to study multiphoton coherent excitation by intense pico-second pulses is presented. The experimental setup includes a dye laser oscillator-amplifier, an interferometric autocorrelator and a computerized data acquisition system.

# INTERFEROMETRIC AUTOCORRELATIONS APPLIED TO THE STUDY OF MULTIPHOTON COHERENCE

H. Vanherzeele and J.-C. Diels  
Center for Applied Quantum Electronics  
Department of Physics  
North Texas State University  
P.O. Box 5368; NT Station  
Denton, Texas 76203  
817-565-3308

We developed a high gain picosecond pulse dye laser oscillator-amplifier system, coupled to an interferometer and a computerized data acquisition system, to perform nonlinear experiments with accurately phased pulse sequences in vapors.<sup>1</sup> Data acquisition and processing is performed on line at the 10 Hz repetition rate of the laser source. The interferometric delay line splits the main pulse into two pairs of pulses with continuously increasing delay. The relative phase between the pulses (slowly increasing at a rate of circa  $2\pi/4s$ ), as well as the absolute delay between the pulses is determined from a HeNe laser interferogram. Our setup, which permits to analyze the waveform and phase modulation of the pulse, is designed to investigate multiphoton coherent effects by cross correlating the multiphoton stimulated re-radiation with the pulse itself.

The ratio of the second harmonic after the interferometer to that before the interferometer, provides both the intensity and interferometric autocorrelation. These measurements enabled us to determine the pulse shape to be  $E = \exp [-(t/5.27)^2 + i\phi]$  with  $\phi = 1.43 E^2$ , and  $t$  in ps.

The other pair of pulses is sent in conditions of multiphoton resonance into a vapor. The second harmonic of the transmitted signal is recorded as a function of the delay and the relative phase between the pulses. The periodicity in phase of the transmitted signal is a direct measurement of the order of the process ( $2\pi$  for single photon,  $\pi$  for two photon,  $\pi/2$  for four photon

resonance). The shape and decay of the signal provides simultaneously information about coherence times as well as spectroscopic information.<sup>2</sup> It should be noted that, because of our accurate knowledge of the pulse shape, our temporal resolution is at least one order of magnitude smaller than the pulse duration (6.2 ps FWHM).

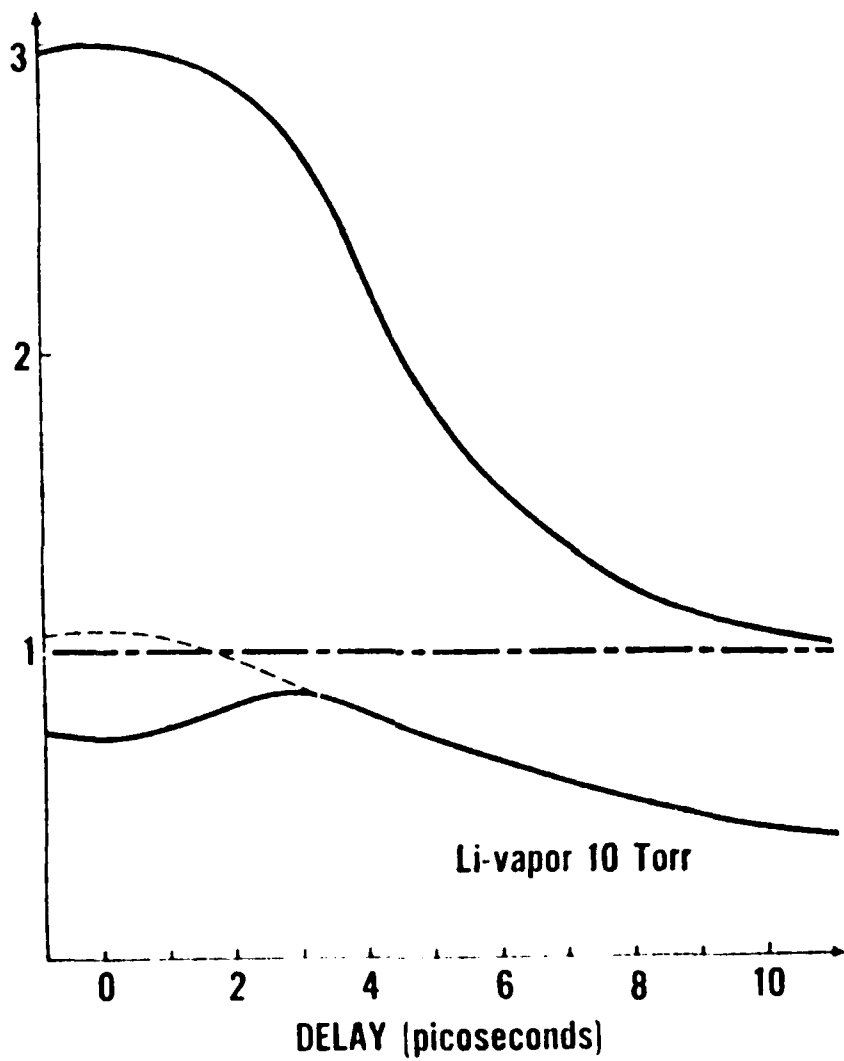
The software of our data acquisition system averages out data over several periods for a given phase, in order to generate an accurate display of signal (or transmission) versus phase. Simultaneously, phase averaged values of the data are also computed. As an example of the latter, the second harmonic of the signal transmitted through Li vapor, as a function of delay between the pulses, is displayed in Fig. 1. The laser pulses are tuned to resonance with the 2s-4s two photon transition of Li at 571.2 nm. In the absence of Li, the averaged data correspond to the conventional 3:1 intensity autocorrelation curve. The enhanced averaged attenuation in Li near zero delay is in perfect agreement with a quantum mechanical calculation of the coherent interaction of the radiation with the two level system. The phase dependent data on the other hand, are much more complex but also richer in information. Examples of coherent interaction in dye vapors (single photon), Li vapor (two photons), and Hg vapor (four photons) will be presented to demonstrate this.

1. H. Vanherzeele and J.-C. Diels, J. Opt. Soc. Am. 73, 1887 (1983).
2. S. Besnainou, J.-C. Diels, and J. Stone, Molecular Multiphoton Excitation by Phase Coherent Pulse Pairs (submitted to J. Chem. Phys.).

Vanherzeele, et. al.

Interferometric Autocorrelations Applied to...

Figure 1. Second harmonic intensity versus pulse delay before (upper trace)  
and after (lower trace) propagation through Li vapor.



END

FILMED

6-84

DTIC

